Chapter IV

Containments for liquids at zero gravity.

(To appear in Applied Microgravity Technology)

G. Smeets
Graduate Aeronautical Laboratory
California Institute of Technology
Mail code: 205-45
Pasadena, CA 91125
U.S.A.

Abstract

A theory proposed by Concus and Finn in 1974 and recently developed by Finn yields explicit geometrical criteria for the position of the free surface of a liquid at zero gravity in a cylindrical container of specified cross section. These criteria were applied by Concus and Finn to three container geometries; the bathtub, the trapezoid, and the keyhole. It is possible to find geometrical criteria that promise a liquid interface of finite height, with the base still covered with liquid, or a liquid interface of infinite height, with the liquid wetting a well defined portion of the wall. In the present work, calculations are presented for a fourth geometry, the non-concentric cylinders. In addition, the earlier calculations of Concus and Finn are extended, and a unified graphical presentation of all four geometries is given that can be used directly for the design of containments for liquids at zero gravity.

1 Introduction

The work reported here was carried out in preparation for a proposed space experiment. The objective was to study the relationship between container geometry and interface geometry for a free liquid surface in equilibrium at zero gravity. The research has involved an analytical and numerical study of the four container geometries shown in Fig. 1. The intent was to determine the shapes of these four geometries for which the liquid location at zero gravity is qualitatively different from that found at non-zero gravity. Three of these configurations, the bathtub, the trapezoid, and the keyhole, were studied previously by Concus and Finn [1, 2] and are discussed here in somewhat more detail. The non-concentric-cylinder geometry was conceived by Coles [3]. Drop-tower experiments conducted to investigate the behavior of liquids in the bathtub geometry are reported in another paper [4]. The results of the experiments encouraged continuation of the analytical study. The results from all four geometries are displayed in a unified graphical representation that indicates different properties of these geometries in a zero-gravity environment.

The paper should be useful to designers of containers and pipes for use at zero-gravity. If the four geometries considered here are not adequate for a particular application, the user can extend the analysis to other geometries of interest. The static theory as developed by Finn [5] is quite general and applies to cylindrical containers of arbitrary cross-section. However, each case must be investigated individually. Dynamic liquid behavior caused by accelerating, emptying, filling, heating, or otherwise disturbing a static situation is not accounted for here. However, information regarding the static equilibrium position of a liquid at zero gravity provides a natural starting point for a study of dynamic behavior.

In general, the location of a liquid in a container at zero gravity is dependent upon the shape of the container and the contact angle γ between the chosen liquid and the container walls. Consider a cylinder of some arbitrary cross section Ω, partially filled with a liquid and standing upright in a normal gravity field, as shown in Fig. 2. A striking feature of the Concus-Finn [6] and Finn [1, 5] theories is the existence of a critical contact angle $\gamma_0(\Omega)$, with $0 \le \gamma_0 \le \frac{\pi}{2}$, such that when $\gamma_0 < \gamma \le \frac{\pi}{2}$ a large enough volume V of fluid will cover the base and yield an

interface of bounded height. When $0 \leq \gamma < \gamma_0$, however, every large enough volume of fluid will rise to the top of the container along a portion of the boundary walls, regardless of container height. If the liquid and the shape of the cross section are chosen appropriately, a liquid that resides on the base of the container in a one-gravity field may reside on a well-defined portion of the walls at zero gravity. The theory is based on a functional Φ, which is derived from the Laplace-Young equation and is described in Section 2. The application of this functional to the four geometries is described in Section 3. Results and conclusions are given in Sections 4 and 5. A detailed discussion of the topology of the graphical results is left to the appendix.

2 Theory

For greater detail on the theoretical background and derivations, the reader is referred to Finn [5]. The theory stated here is only what is necessary for the present discussion.

Let a standard variational technique be used to minimize an expression for the free energy of a liquid in a container at zero gravity. The free energy includes the free surface energy ($E_S = \sigma S$) and the wetting energy ($E_{S^*} = -k_0 \sigma S^*$), where σ is the surface tension, S and S^* are the free surface area of the interface and the wetted surface area of the container, respectively, and k_0 is a constant of proportionality. The total volume of the liquid is held constant as a constraint, represented by a term $k_1 V$. Thus

$$E(S) = S - k_0 S^* + \frac{k_1}{\sigma} V \tag{1}$$

Minimization of the free energy defined by Eqn. (1) yields the Laplace-Young equation for a static liquid free surface in a cylinder of arbitrary cross section at zero gravity;

$$\text{div } T(u) = \frac{\Sigma \cos \gamma}{\Omega} \tag{2}$$

$$\mathbf{n} \cdot \mathbf{T}(u) = \cos\gamma = k_0 \tag{3}$$

where $\mathbf{n}$ is the unit outward normal, Σ and Ω are the perimeter and area of the cross section, γ is the contact angle measured in the liquid, $u = u(x,y)$ is the height of the free surface, and

$$\mathbf{T}(u) = \frac{\nabla u}{(1 + |\nabla u|^2)^{1/2}} \tag{4}$$

Consider a cross section of the container, normal to the axis, as sketched in Fig. 3. Assume that the free surface intersects the cross section along a curve Γ. Integration of Eqn. (2) over this section yields an energy per unit length defined by

$$\Phi(\Gamma) = \Gamma - (\cos\gamma)\Sigma^* + \left[\frac{\Sigma\cos\gamma}{\Omega}\right]\Omega^* \tag{5}$$

which is a two-dimensional analog to the three-dimensional energy defined by Eqn. (1) [1]. There is a close analogy between the free surface area S, the wetted surface area S^*, and the liquid volume V in Eqn. (1) and the length of the curve Γ, the length of the wetted boundary Σ^*, and the liquid area Ω^* in Eqn. (5).

The cylinder has a flat bottom Ω and a smooth boundary Σ, while Γ is a circular arc of radius $R_\gamma = \frac{\Omega}{\Sigma\cos\gamma}$ for the entire range $0 \le \gamma \le \frac{\pi}{2}$. Under these circumstances, the liquid surface extends to a finite height inside the cylinder if and only if $\Phi > 0$ for every arc Γ that can be drawn in the cross section such that the arc meets the walls at the contact angle γ. In general, there are at most a finite number of these arcs that can be drawn; therefore, it is sufficient to evaluate Φ for only a finite number of cases. For the critical contact angle γ_0 introduced above, there will be at least one arc Γ such that $\Phi = 0$, with $\Phi \ge 0$ for all other arcs. In the present work, the aim is to determine these critical arcs Γ, since they separate the two types of behavior described below.

Whenever $\Phi > 0$ on all arcs Γ, the height of the liquid interface is bounded. To be precise, a solution $u(x,y)$ exists for the Laplace-Young equation (Eqns. (2)-(4)). The surface defined by $u(x,y)$ minimizes the mechanical energy among all possible surfaces satisfying the prescribed

volume constraint and meeting the bounding walls of the container at the contact angle γ.

Whenever $\Phi = 0$ for some arc Γ, a bounded solution cannot be found. The mechanical energy is then formally minimized by a generalized function that is positive infinite in Ω^* and finite in the rest of the domain, or finite in Ω^* and negative infinite in the rest of the domain. In the real case, this conclusion means infinite liquid rise (or rise to the top of the container) in Ω^* and possible uncovering of the base outside Ω^*, depending upon the volume of available liquid. It is this behavior that can be inferred from the graphical descriptions for the four cases discussed here.

3 Application of theory

Application of the Φ functional, described in section 2, to a particular geometry requires that all the terms in the functional be defined for that geometry. A position for the circular arc Γ must be specified in order to determine Σ^* and Ω^*. This circular arc represents the position of the free surface of the liquid in the cross section; therefore, the arc must meet the walls at the contact angle. Each geometry considered here requires special attention to details to determine the terms in Φ, which are listed in Figs. 4a-4e. It is useful to refer to the drawings of each geometry given in Figs. 5-8 for the following discussion.

Finn [1] presented a detailed account of the procedure used to find the location of the critical circular arc Γ for the trapezoid cross section. He considered all possible positions of Γ and found that $\Phi > 0$ for all except two of these. Fig. 6 shows that one of these arcs Γ is symmetrically located on the long-axis centerline, with the convex side of the arc toward the narrow end of the trapezoid. The other arc Γ is located in the corners of the trapezoid, with the convex side toward the corner, indicating the possibility of liquid rise to infinity there. Critical behavior of liquids in corners is considered again in the discussion of the bathtub and the trapezoid in the appendix.

The location of the arc Γ for the bathtub cross section shown in Fig. 5 was also determined by Finn [7]. A general rule appears to be that the liquid tends to rise in regions of higher curvature or in the narrower end of the container. When applied to the keyhole cross section,

this rule yields Γ as shown in Figs. 7a and 7b [8]. The cross section for the non-concentric cylinders is rather different from the other three, but application of the rule yields two circular arcs positioned as shown in Fig. 8a. Although this general rule is simple, finding critical solutions with $\Phi = 0$ is positive proof of correct arc placement. If the arc is not correctly placed, it is always found that $\Phi > 0$ [8].

When a general position for the arc Γ has been found, the geometric expressions for the terms of the Φ functional can be determined. The terms for each geometry include those listed in Figs. 4a-4e and the following equations, which are common to all four geometries:

$$R_\gamma = \frac{\Omega}{\Sigma \cos\gamma} \tag{6}$$

$$\Gamma = 2\theta R_\gamma \tag{7}$$

Eqn. (6) represents the radius of the circular arc Γ and Eqn. (7) represents its length. It is necessary to double the right-hand side of Eqn. (7) for the non-concentric cylinders, because there are two circular arcs. Each geometry is fully defined by two parameters α and β, which are shown in Fig. 1 for each geometry. The parameter α is defined as the half angle of the extended sides or tangents, with the exception of the non-concentric cylinders. For the latter, α is the angle between the axis of symmetry of the cross section and the line segment connecting the tops of the two circles. The parameter β is always defined as the ratio of the radii or sides, with the larger radius or half height defined to have unit length. These definitions for α and β allow the full range of possible shapes of each geometry to be represented by a finite range for each parameter, $0 \le \beta \le 1$ and $0° \le \alpha \le 90°$. The functional Φ depends only on geometry and contact angle. Therefore, $\Phi = \Phi(\alpha, \beta, \gamma)$.

In addition to choosing uniform geometric parameters to represent each geometry, the equations in Figs. 4a-4e have been written in a consistent form. For example, the total perimeter Σ is always written such that the first term represents the perimeter of the left portion or narrow end of the cross section. The second term represents the perimeter of the middle portion, and the last term represents the perimeter of the right portion. In the case of the

keyhole without parallel sides, pictured in Fig. 7b, and in the case of the non-concentric cylinders, pictured in Fig. 8a, there is no middle portion, but the left and right portions are represented in the standard way. The same is true for the organization of the rest of the expressions. The quantity θ always represents the half angle subtended by the arc Γ. The quantity ϕ is used for the keyhole with $h < 0$ in Fig. 7b and for the non-concentric cylinders in Fig. 8 to represent the angle of β from the center line to the intersection of the arc Γ with the cross section. The quantity λ represents the center-to-center distance in Figs. 5-8. For the bathtub in Fig. 5 and the trapezoid in Fig. 6, δ represents the distance of the circular arc Γ from the small end of the cross-section. The quantity h is introduced with the keyhole geometry in Figs. 7a and 7b to represent the length of the parallel sides. If no parallel sides are present, h is considered to be non-positive.

The terms for the bathtub and the trapezoid were determined by straightforward application of geometrical identities. These terms were given explicitly by Finn [1, 7]. The terms listed in Figs. 4a and 4b correspond exactly to Finn's notation; however, they are written in a form chosen for consistency among the four geometries considered here.

The keyhole geometry has two distinct shapes. Fig. 7a shows the case where the cross section contains parallel sides and Fig. 7b shows the case without parallel sides. The length of the parallel sides is defined as h. The keyhole terms for the case $h > 0$ are listed in Fig. 4c. The terms for the keyhole with $h < 0$, listed in Fig. 4d, are slightly more complicated. For the case $h = 0$, either set of equations can be used. The loss of the parallel sides requires the introduction of the point (X,Y), indicated in Fig. 7b, where the large circle intersects the smaller one. For the keyhole geometry, the arc Γ is located at the reentrant corners of the cross section, and does not change position with contact angle or container shape. However, the radius and the length of Γ still vary according to Eqn. (6) and (7). Theorem 1 of Finn [5] states that the arc Γ must intersect the reentrant corners and need not meet the walls at the contact angle γ; in fact, the angle between Γ and the parallel sides is $\geq \gamma$.

The terms for the non-concentric cylinders, shown in Fig. 4e, are the most complex among the four geometries. In this case, the two points of intersection, indicated in Fig. 8b, between Γ and the cross-section had to be numerically determined. X1 and X2 were iterated until the

circular arc Γ met the inner and outer cylinders at the contact angle γ. This additional complication yields the five-term expression for Ω^* given in Fig. 4e. The first term, Θ, is the area of the entire sector of the larger cylinder that contains the arcs Γ in Fig. 8a. The next four terms represent areas of the corresponding sections labeled 1 through 4 in Fig. 8b. Note that the areas in Fig. 8b must all be doubled to represent the areas on both sides of the dashed centerline.

The terms for Φ were inserted into computer programs for each geometry. The critical values $\Phi(\alpha, \beta, \gamma) = 0$ were found by straightforward application of binary search and secant-method zero-finding algorithms. The location of the arc Γ for the bathtub, the trapezoid, and the keyhole was found by straightforward analytical means once the contact angle γ was specified. The location of the arc Γ for the non-concentric cylinders, however, was found by iterating X1 and X2 (Figs. 4e, 8a). For all geometries, $\gamma = \gamma_0$ was chosen, β was fixed, and α was searched to find $\Phi(\alpha, \beta, \gamma_0) = 0$; then β was changed, and α was searched again. In every case, zeros of Φ were found to an accuracy of 10^{-12} or better using double-precision calculations.

4 Results

The results for each geometry are given in graphical form in Figs 9-12. The abscissa in every plot is $0° \le \alpha \le 90°$ and the ordinate is $0 \le \beta \le 1$, where α and β are the geometric parameters for each cross section. A particular geometry is fully defined by choosing a point (α, β). The first plot in each case, namely Figs. 9a, 10a, 11a, and 12a, depicts the critical curves $\Phi(\alpha, \beta, \gamma_0) = 0$ for γ_0 = constant. Any geometric point (α, β) lying on a particular curve $\Phi(\alpha, \beta, \gamma_0) = 0$ is critical for contact angles $\le \gamma_0$. That is, liquid rises to infinity on the convex side of the arc Γ at zero gravity. The second plot, namely Figs. 9b, 10b, 11b, and 12b, displays dotted curves of constant critical area ratio. For all the geometries except the non-concentric cylinders, the critical area ratio A_{crit} is defined as the ratio of cross sectional area occupied by liquid to the total available cross sectional area; i.e., $\frac{\Omega^*}{\Omega}$. For the non-concentric-cylinders case, $A_{crit} = \frac{\Omega^*}{\pi}$, where π is the area of the larger cylinder. If Ω is used rather than π,

$A_{crit} \approx$ 100 percent is found as $\beta \rightarrow 1$, yet almost no liquid is contained in the very small space between the two cylinders. The third plot, namely Figs. 9c, 10c, 11c, and 12c, depicts curves λ = constant. The quantity λ represents the center-to-center distance or, in the case of the trapezoid, the end-to-end distance. For all the geometries except the non-concentric cylinders, λ has a full range from zero to infinity. For the non-concentric cylinders case, λ is restricted to $0 \leq \lambda \leq 1$, otherwise the inner cylinder would protrude beyond the outer one. Note that all the curves in Figs. 9-12 are labeled from right to left except Fig. 12b, which is labeled in the reverse order.

For every plot shown, the computed points are connected by straight line segments. No curve fits were employed to smooth the computed data points; therefore, individual computed points are not shown. The computations yielded points (α, β) for a given γ_0 such that $\Phi(\alpha, \beta, \gamma_0) = 0$. Curves of A_{crit} = constant were determined by interpolating the A_{crit} results for each curve $\Phi(\alpha, \beta, \gamma_0) = 0$. For this purpose, various additional curves were computed for intermediate values of γ_0 in order to yield smooth critical area-ratio curves. Curves λ = constant were computed from the geometrical formulas shown in Figs. 4a-4e.

Each of the following four parts discusses the plots for a particular cross section. A number of prominent features that warrant close attention are discussed in the appendix.

Bathtub: The graphical results for the bathtub geometry are shown in Figs. 9a-9c. The design point for the container used in experiments at the NASA Lewis drop-tower facility [4] is indicated on each plot. As previously stated, the results of these experiments encouraged the continuation of this work.

Critical curves $\Phi = 0$ for $\gamma = 0°(5°)85°$ are shown in Fig. 9a. A similar plot for this geometry was presented by Concus and Finn [2], who plotted γ versus β with α constant. The points along each curve in Fig. 9a were found for a particular $\gamma = \gamma_0$ by first fixing β and then scanning the α range. This procedure yielded more than one zero for Φ; however, inspection revealed that $\delta < 0$ for all of these except one. The given formulas for Φ in Fig. 4a consider only the intersection of Γ with the non-parallel sides; therefore, $\delta < 0$ is not valid in this context. When the terms of Φ were written to include intersection of the curve Γ with the small

circular end, no zeros were found. The convergence of the curves $\Phi = 0$ to the point $\alpha = 0°$, $\beta = 1$, the α-intercepts, and the curve for $\gamma_0 = 0°$ are discussed in the appendix.

The curves are more easily understood by an application, in this case to the drop-tower experiments [4]. The plexiglas containers for these experiments were designed to have a critical contact angle of 30° with $\beta = 0.5$. Fig. 9a shows that the design point lies on the curve $\Phi = 0$ for $\gamma_0 = 30°$. The design point lies below and to the left of all critical curves for which $\gamma_0 < 30°$, and lies to the right and above all critical curves for which $\gamma_0 > 30°$. If a liquid partially filling this container has a contact angle of 30° or less, it will attempt to rise to infinity in the narrow end of the cross section. This behavior was seen in the experiments when 50% ethanol in water ($\gamma_0 \approx 23°$) was used. If the liquid has a contact angle greater than 30°, it rises to a finite height [6, 9]. This behavior was seen for water ($\gamma_0 \approx 72°$) and for 10% ethanol in water ($\gamma_0 \approx 55°$).

Plots of A_{crit} = constant and λ = constant for the bathtub geometry are shown in Figs. 9b and 9c respectively. The curves in Fig. 9b are bounded above by the curve $\gamma_0 = 0°$. The curves λ = constant depict how the center-to-center distance changes with the geometric parameters. The design point for the drop-tower tests had $A_{crit} \approx 12$ percent with $\lambda \approx 5$. For the design, it was important to have a sizeable percentage of the cross section filled with liquid while at the same time restricting the container to a reasonable length.

Trapezoid: The graphical results for the trapezoid geometry are shown in Figs. 10a-10d. Unlike the other three geometries, corners are always present in this cross section (Fig. 4b). The presence of corners complicates the explanation of the results. Basically, critical liquid rise in the corners is not as large-scale as it is in the narrow end of the container, and both can occur for the same contact angle and geometry. The curves $\Phi = 0$ in Fig. 10a are interpreted in the same manner as for the bathtub geometry. In this case, each scan of α for fixed β yielded only one zero for Φ. Some prominent physical features, such as the α-intercepts and the convergence of the curves $\Phi = 0$ to the point $\alpha = 0$, $\beta = 1$ were also seen for the bathtub geometry. The dotted and dashed curves in Fig. 10a, along with the fact that some of the curves $\Phi = 0$ end in mid-plot, are discussed in the appendix. The curves of A_{crit} = constant in Fig. 10b and λ = constant in Fig. 10c are once again easily understood. To obtain a higher

percentage of the cross section filled with liquid, it is necessary to consider longer lengths. The plot of curves $\delta = 0$ shown in Fig. 10d is discussed in the appendix.

Keyhole: The results for the keyhole geometry are shown in Figs. 11a-11c. The curves $\Phi = 0$ are interpreted in the same way as the previously discussed geometries. Only one zero was found for Φ for a given scan of α. The dashed curve in Fig. 11a indicates where $h = 0$. A different set of equations is used for the terms of the Φ functional for $h > 0$ and for $h < 0$ (Figs. 4c, 4d). The solutions join smoothly. The convergence of the curves $\Phi = 0$ to the point $\alpha = 90°$, $\beta = 0$, the β-intercepts, and the curve $\gamma_0 = 0°$ are discussed in the appendix. The interpretation of the curves A_{crit} = constant in Fig. 11b and the curves λ = constant in Fig. 11c is straightforward. The curves in Fig. 11b are bounded above by the curve for $\gamma_0 = 0°$ and bounded below by the curve for $\gamma_0 = 89.9°$. Note that critical area ratios larger than 30% are possible for reasonable values of λ and β.

Non-concentric cylinders: The graphical results for the non-concentric cylinders are given in Figs. 12a-12c. This set of plots differs markedly from the others considered here. The α range ($45° \le \alpha \le 90°$) is half of the α range seen for the three previous geometries. This limitation is a physical consequence of the geometry; at $\alpha = 45°$, the inner cylinder touches the wall of the outer cylinder. To allow α to go beyond this value would involve the consideration of crescent-shaped domains. The other distinguishing features are discussed in the appendix.

The curves $\Phi = 0$ in Fig. 12a are interpreted differently from the curves $\Phi = 0$ for the other geometries. If a point (α, β) lies to the right and below a particular $\gamma = \gamma_0$ curve, a liquid with a contact angle γ_0 would rise to a finite height in the container. However, if (α, β) lies on or above the curve, a liquid with that contact angle would rise to infinity. The technique used to find zeros for this geometry did not yield results for $\gamma_0 = 0°$. The curve for $\gamma_0 = 1°$ is plotted, and overlaps the curve for $\gamma_0 = 5°$. It is supposed that the curve for $\gamma_0 = 0°$ would also overlap. The curves A_{crit} = constant in Fig. 12b and the curves λ = constant in Fig. 12c are easily understood as before. The curves in Fig. 12b are bounded below by the curves for $\gamma_0 = 1°$.

5 Discussion and Conclusions

In the containers discussed above, the liquid tends toward the narrow ends or areas of high curvature at zero gravity. In the limit $\beta \rightarrow 0$ the small end of the bathtub or the trapezoid becomes a corner of angle 2α and the corner-condition [6] is satisfied by the curves $\Phi = 0$ (see the appendix). In the limit $\beta \rightarrow 1$ the sides of the bathtub and the trapezoid become parallel and all the curves $\Phi = 0$ converge to $\alpha = 0°$.

All of the plots in Figs. 9a, 10a, 11a, and 12a have empty regions. In Figs. 9a, 10a, and 11a, a geometry (α, β) effects finite liquid rise for a particular contact angle γ_0 if it is located above and to the right of the curve $\gamma = \gamma_0$. In Fig. 12a, a geometry (α, β) effects finite rise if it is located below and to the right of the curve. Therefore, any geometry (α, β) located in the blank region of a plot will not effect infinite rise for any contact angle. The results of Bainton [9] for the bathtub show that the farther the design point is above a curve $\Phi(\alpha, \beta, \gamma_0) = 0$, the smaller the finite rise height. For the keyhole, this blank region encompasses nearly the entire upper half of the plot. A designer of such a geometric shape for use in zero gravity might be disappointed with the results if β were chosen to be larger than 0.506 and large liquid rise was desired.

Another practical consideration for designing containers is the actual value of the contact angle. The contact angle depends on the liquid and the material chosen for the container. It also depends upon surface cleanliness, liquid purity, and other properties, such as surface roughness. Note that all the work presented here also applies to contact angles larger than 90° by using the supplement of the angle and considering the accompanying fluid as the one that is producing the movement. Consider vapor over a liquid with a contact angle of 120°. If the container is designed to have a critical angle of 60° or more, then the vapor would try to occupy the area of the container on the convex side of the arc Γ. In many applications, cleanliness and purity may not be fully controllable, or the contact angle may not be known. A conservative designer could choose a container shape that is critical for a large range of contact angles. For the bathtub, the trapezoid, and the keyhole, the designer might choose to design for a critical contact angle of 80°. This choice, although yielding a rather long cross section, will effect infinite liquid rise for liquids with contact angles less than or equal to 80°. For the non-

concentric cylinders, the designer need not know the contact angle. For example, with $\beta = 0.5$ and the inner and outer cylinder concentric ($\alpha = 90°$) small finite rise should occur for any liquid with $\gamma < 90°$. As the inner cylinder is moved radially ($\alpha \rightarrow 45°$), the liquid will rise to infinity as the appropriate critical curve is crossed. Used this way, the non-concentric cylinders could conceivably be used for measurement of the contact angle. This geometry also presents a means of causing fluid to move on demand, by merely moving the cylinder radially to effect liquid rise and then back toward the concentric position to cause the liquid to fall again. This geometry is the only one of the four considered here for which it is easy to visualize a continuous variation of the geometric parameters as part of an experiment in space.

If $\gamma_0 = 90°$, then the liquid has no component of surface tension along the solid surface of the container. Thus no liquid motion would be expected. All four geometries considered here demonstrate this rather vividly. Consider the bathtub. In the limit $\gamma_0 \rightarrow 90°$, Fig. 9a suggests that the curve $\Phi = 0$ approaches the left edge of the plot. In order for a geometry (α, β) to be critical, for $\gamma = \gamma_0$, it must be located below and to the left of the curve $\Phi(\alpha, \beta, \gamma_0) = 0$. However, this condition becomes increasingly difficult to satisfy as $\gamma_0 \rightarrow 90°$. At $\gamma_0 = 90°$, all the geometries in the plot are non-critical. This property is also seen in Figs. 10a, 11a, and 12a.

For other applications, the amount of liquid that rises may be important. For this purpose, the plots of A_{crit} = constant provide a useful guide. The user should be aware that these critical area-ratios are for the critical case only, that is to say that if the design point (α, β) is located on a curve $\gamma = \gamma_0$, then this area ratio is valid for a liquid with contact angle γ_0. These values of A_{crit} were interpolated from results for $\Phi = 0$ for many curves $\gamma = \gamma_0$. If a large region of liquid rise is desired, the designer should choose (α, β) within the highest A_{crit} contour on the curve $\gamma = \gamma_0$ of interest. It is worth noting that both the keyhole and non-concentric cylinders have finite A_{crit} values along their respective curves $\gamma_0 = 0°$, whereas $A_{crit} = 0$ along the curve $\gamma_0 = 0°$ for the bathtub geometry. Each of the containers considered here easily offers $A_{crit} \simeq 20$ percent for reasonable values of λ and β. Higher percentages can be realized with the keyhole geometry. However, this is simply a matter of making the parallel section longer so that it comprises a larger percentage of the cross sectional area. The result is a rather long container that may or may not be convenient for certain applications.

The results presented above provide a starting point for designers of containments for liquids at zero gravity. While these results do not settle dynamic questions, they do provide workable criteria in the four cases discussed, in order that statically stable configurations can be achieved. The theories of Concus and Finn [6] and of Finn [1, 5], on which the above work is based, can in principle be applied in analogous ways to cylindrical containers of arbitrary cross section.

This material is based upon work supported by the U.S. National Aeronautics and Space Administration and the University of California. I am indebted to D. Coles, P. Concus, and R. Finn for useful discussions. The opinions, findings, conclusions and recommendations are those of the authors and not necessarily of the U.S. National Aeronautics and Space Administration or the University of California.

Appendix

Some details regarding the topology of the plots in Figs. 9a, 10a, 11a, and 12a are presented below for each geometry. In addition, a discussion of the curves $\delta = 0$ in Fig. 10d is included in the trapezoid section.

Bathtub: All the curves $\gamma = \gamma_0$ shown in Fig. 9a intersect α-axis at $\alpha = 90° - \gamma_0$. The case $\gamma_0 = 0°$ is not so obvious and is discussed below. In addition, the slope of the curves $\Phi = 0$ at the intercepts is identically zero for all γ_0.

$$\frac{\partial\beta}{\partial\alpha} = \frac{1 - (\sin^2\gamma + \cos^2\gamma)}{4\cos\gamma\,(\sin\gamma - \gamma\cos\gamma)} \tag{8}$$

Explanation requires attention to the shape of the cross section as these intercepts are approached. In the limit $\beta \rightarrow 0$, the small end of the bathtub becomes a corner of angle 2α. Concus and Finn [6] determined that if $\alpha + \gamma < 90°$ the liquid free surface rises to infinity in the corner indicated in Fig. 13. Fig. 9a indicates that if $\beta = 0$ and $\alpha + \gamma_0 \leq 90°$ the liquid rises to infinity in the corner. Concus and Finn [6] also state that Γ is coincident with the corner. This is equivalent to $\delta = 0$, $R_\gamma = 0$ as found numerically.

The curve $\gamma_0 = 0°$ intersects the right side of the plot at $\alpha = 90°$, $\beta = 0.5$. This result seems curious when compared to the other curves on the plot. Analytically, setting $\gamma = 0°$ in the Φ terms listed in Fig. 4a and substituting them into Eqn. (5) with $\Phi = 0$ yields:

$$\Phi = \frac{(T - \beta)^2}{T}\left[\left(\frac{\pi}{2} - \alpha\right) - \cot\alpha\right] \tag{9}$$

where

$$T = \frac{R_\gamma \sin\left(\frac{\pi}{2} - \gamma - \alpha\right)}{\cos\alpha} = R_\gamma \tag{10}$$

since $\gamma = 0°$. Substitution of Eqn. (10) into Eqn. (9) yields:

$$\Phi = \frac{(R_\gamma - \beta)^2}{R_\gamma}[(\frac{\pi}{2} - \alpha) - \cot \alpha] \tag{11}$$

Thus $\Phi = 0$ implies $\cot \alpha = (\frac{\pi}{2} - \alpha)$ and/or $R_\gamma = \beta$. The first case yields $\alpha = \frac{\pi}{2}$, or the entire right side of the plot, since this result is not limited in β. The second case yields the equation

$$\cot \alpha = (\frac{\pi}{2} - \alpha) - \frac{\pi(1 - 2\beta)}{(1 - \beta)^2} \tag{12}$$

Note that at $\beta = 0.5$ this case reduces to the first one. Hence the intercept at $\alpha = 90°$, $\beta = 0.5$. The curve $\gamma_0 = 0°$ shown in Fig. 9a was computed using Eqn. (12). Note that because $T = R_\gamma = \beta$, and $\delta = 0$, the arc Γ is coincident with the circular arc of radius β.

All the curves $\Phi = 0$ converge at the point $\alpha = 0$, $\beta = 1$. The case $\beta = 1$ was studied by Concus and Finn [6] as a possible candidate for an "astronaut's bathtub". In the limit $\beta \rightarrow 1$, α necessarily goes to zero, since $\beta = 1$ requires parallel sides. This property was also discussed by Concus and Finn [2].

Trapezoid: All the curves $\gamma = \gamma_0$ shown in Fig. 10a intersect the α-axis at $\alpha = 90° - \gamma_0$, and at zero slope. This behavior was also exhibited by the curves for the bathtub in Fig. 9a. The explanation for this behavior is given above in the bathtub section of this appendix. The analytic expression for the slope at these points is:

$$\frac{\partial \beta}{\partial \alpha} = \frac{(1 - (\sin^2\gamma + \cos^2\gamma))^2}{2\sin 2\gamma} \tag{13}$$

The dotted curve in Fig. 10a indicates the point, along a given curve $\gamma = \gamma_0$, where the acute corners become critical. Define α_0 as the α at which the dotted curve crosses a particular curve $\gamma = \gamma_0$. Infinite liquid rise is expected to occur in the acute corners for $\alpha > \alpha_0$ along a particular curve $\gamma = \gamma_0$. Therefore, for $\gamma_0 \leq 45°$ the plot shows that the acute corners are critical for all α, and for $\gamma_0 > 60°$ the acute corners are not critical along the $\gamma = \gamma_0$ curves.

The dashed curve in Fig. 10a indicates the point, along the curve $\gamma = \gamma_0$, where the obtuse corners become critical. Once again define α_0 as the value of α at which the dashed curve

intersects a particular curve $\gamma = \gamma_0$. In this case, for all $\alpha < \alpha_0$ along a particular curve $\gamma = \gamma_0$, the liquid rises to infinity in the obtuse corners. For the critical curve $\gamma = 30°$, for example, this rise occurs for $\alpha \leq 30°$. If $\gamma > 45°$ then the obtuse corners do not become critical.

It is important to note that the dotted and dashed curves described above do not define regions of the (α, β) plot where the acute and obtuse corners become critical. They only act as indicators as to where these corners become critical along the curves $\gamma = \gamma_0$. General regions of corner criticality can be defined. However, these regions are bounded by vertical lines on an (α, β) plot. This corner condition is independent of β except for the case $\beta = 0$, where the two obtuse corners merge to become one corner of angle 2α. The acute corners are critical if $\alpha \geq (2\gamma - 90°)$, and the obtuse corners are critical if $\alpha \leq (90° - 2\gamma)$. Consider the acute corners first. If $\gamma = 45°$, then the acute corners are critical for all $\alpha \geq 0°$. If $\gamma < 45°$, then $\alpha \geq$ (negative value), but $0° \leq \alpha \leq 90°$. Therefore, the acute corners are critical for all valid α. For example, if $\gamma = 30°$, then $\alpha \geq -30°$, and the acute corners are critical for $-30° \leq \alpha \leq 90°$ and for $0 \leq \beta \leq 1$ as shown in Fig. 14a. If $\gamma > 45°$, then the area of criticality begins to shrink. For example, Fig 14b shows the critical region for $\gamma = 60°$. Critical liquid rise occurs in the acute corners when $(2\gamma - 90°) \leq \alpha \leq 90°$ for $0 \leq \beta \leq 1$.

Infinite liquid rise occurs in the obtuse corners when $0° \leq \alpha \leq (90° - 2\gamma)$ for $0 < \beta \leq 1$, as shown in Fig. 14c. Immediately noticeable is the fact that for $\gamma \geq 45°$ the obtuse corners are never critical. At $\beta = 0$ the obtuse corners no longer exist, and are replaced by one corner of angle 2α. If $\alpha + \gamma \leq 90°$, then infinite rise occurs in this corner. The region of the (α, β) plot that has infinite rise in the obtuse corners, and also in the corner 2α, is $0 \leq \alpha \leq (90° - 2\gamma)$ for $0 < \beta \leq 1$ and $0 \leq \alpha \leq (90° - \gamma)$ for $\beta = 0$ as shown in Fig. 14c. Fig. 14d demonstrates that all corners can be critical for some contact angles.

Some of the curves $\gamma = \gamma_0$ end in mid plot in Fig. 10a. Calculation of $\Phi = 0$ was stopped when $\delta = 0$. This is the point at which the circular arc Γ makes contact with the small side of the trapezoid (2β). Note that this endpoint always occurs at an α that is less than the critical α_0 for obtuse corners for that particular curve $\gamma = \gamma_0$. As α decreases and β increases along a curve $\gamma = \gamma_0$, the circular arc Γ moves closer to the small end of the trapezoid $(\delta \rightarrow 0)$. At some point (α_0) the obtuse corners, which are already filled with the liquid on the convex side of Γ, become

critical. Presumably nothing spectacular happens as α_0 is crossed. However, as α reaches $\alpha_{endpoint}$, the arc Γ touches the small end and it is no longer possible to draw this particular circular arc. This solution must therefore collapse and the liquid would remain trapped in the obtuse corners for any $\alpha < \alpha_{endpoint}$ for $0 \le \beta \le 1$. If β is decreased, as shown in Fig. 15, with $\alpha = \alpha_{endpoint}$, the arc Γ may reappear.

The plot of curves $\delta = 0$ is shown in Fig. 10d. These curves represent values of α and β, for a given $\gamma = \gamma_0$, for which the arc Γ touches the smaller end (2β) of the trapezoid. The curve $\delta = 0$, for a specific γ_0, intersects the curve $\Phi = 0$ for the same γ_0, at $\alpha = \alpha_{endpoint}$. Note that $\alpha_{endpoint} = 90°$ and $\beta = 0$ for $\gamma_0 = 0°$.

Keyhole: In the limit $\alpha \to 0°$, the curves $\Phi = 0$ in Fig. 11a meet the β-axis at well defined points. In the limit as $\alpha \to 0°$, $h \to \infty$. Therefore, a perturbation expansion of the Φ terms shown in Fig. 4c for large h yields (to leading $O(h^2)$):

$$\Phi = 4\beta^2(\theta + \sin\gamma\cos\gamma) + 4\cos^2\gamma[(\pi - \Theta)(2\beta - 1) - \beta\cos\Theta] \tag{14}$$

$$\theta = (\frac{\pi}{2} - \gamma) \quad ; \quad \Theta = \arcsin(\beta) \tag{15}$$

This set of equations was used to determine the values shown in Table 1 for the β-intercepts. Finn [8] reported a critical radius ratio for $\gamma = 0°$ of $\rho_0 = \frac{1}{\beta} = 1.974$ that is in agreement with the result quoted in Table 1.

All of the curves $\Phi = 0$ converge to $\alpha = 90°$ in the limit $\beta \to 0$. Unlike the two previous geometries, no corner is formed when $\beta \to 0$; therefore, no corner-condition α-intercepts are found. In the limit $\alpha \to 90°$, the cross-section becomes a circle; $h \to 0$ and $\beta \to 0$. The curve for $\gamma = 0°$ intersects the right side of the plot at $\beta = 0.5$. Unlike the other cases, the functional Φ did not cross zero for the case $\gamma = 0°$, instead Φ reached a maximum at $\Phi = 0$. The curve shown is flat from the β-intercept ($\alpha = 0°$), to the dashed $h = 0$ curve. From there, it drops off monotonically to the intercept on the right side of the plot. In the limit $\alpha \to 90°$ for $\gamma = 0°$, the shape of the cross section approaches a circle; therefore, Eqn. (6) yields $R_\gamma = 0.5$. In the limit

$R_\gamma \rightarrow 0.5$, with $\gamma = 0°$. $\beta \rightarrow 0.5$ so that the circular arc of radius β is coincident with the arc Γ.

Non-concentric cylinders: All the curves $\Phi = 0$ in Fig. 12a converge to $\alpha = 90°$ at $\beta = 1$ and to $\alpha = 45°$ at $\beta = 0$. As the inner cylinder radius approaches the outer one ($\beta \rightarrow 1$), no room is left to move the inner cylinder. Hence α must go to 90°. In the limit as $\alpha \rightarrow 45°$, the inner cylinder shrinks to zero radius at the wall of the outer cylinder.

References

[1] *Finn, R.:* Existence criteria for capillary free surfaces without gravity. Ind. Univ. Math. J. **32**(3), 439-460 (1983)

[2] *Concus, P., Finn, R.:* Continuous and discontinuous disappearance of capillary surfaces, in: Variational Methods for Free Surface Interfaces. *Concus, P., Finn, R.* (Eds.), Springer-Verlag, New York, Berlin, p. 197-204 (1987)

[3] *Coles, D.:* Private communication (1986)

[4] *Smedley, G.:* Preliminary drop tower experiments on liquid-interface geometry in partially filled containers at zero gravity. To appear in Experiments in Fluids **8** (1990)

[5] *Finn, R.:* A subsidiary variational problem and existence criteria for capillary surfaces. J. Reine Angew. Math. **353**, 196-214 (1984)

[6] *Concus, P., Finn, R.:* On capillary free surfaces in the absence of gravity. Acta Math. **132**, 177-198 (1974)

[7] *Finn, R.:* Private communication (1985)

[8] *Finn, R.:* Equilibrium capillary surfaces. Springer-Verlag, New York, Berlin, 1986

[9] *Bainton, M.C.:* Fluid interfaces in the absence of gravity. Masters Thesis, Department of Mathematics, Lawrence Berkeley Laboratory, University of California, (1986)

Figure Captions

Figure 1: Four container cross sections

Figure 2: Generic cylinder

Figure 3: Cross section of generic cylinder

Figure 4a: Φ terms: bathtub

Figure 4b: Φ terms: trapezoid

Figure 4c: Φ terms: keyhole, $h > 0$

Figure 4d: Φ terms: keyhole, $h < 0$

Figure 4e: Φ terms: non-concentric cylinders

Figure 5: Bathtub

Figure 6: Trapezoid

Figure 7a: Keyhole, $h > 0$

Figure 7b: Keyhole, $h < 0$

Figure 8a: Non-concentric cylinders

Figure 8b: Non-concentric cylinders: detail of Ω^*

Figure 9a: Critical curves: bathtub [$\gamma = 0°(5°)85°$]

Figure 9b: Critical area-ratio curves: bathtub [$A_{crit} = .01, .05(.05).30$]

Figure 9c: Curves of λ = constant: bathtub [$\lambda = .1, .5, 1(1)10$]

Figure 10a: Critical curves: trapezoid [$\gamma = 0°(5°)85°$]

Figure 10b: Critical area-ratio curves: trapezoid [$A_{crit} = .01, .05(.05).30$]

Figure 10c: Curves of λ = constant: trapezoid [$\lambda = .1, .5, 1(1)10$]

Figure 10d: Curves of $\delta = 0$: trapezoid [$\gamma = 0°(5°)85°$]

Figure 11a: Critical curves: keyhole [$\gamma = 0°(5°)85°$]

Figure 11b: Critical area-ratio curves: keyhole [$A_{crit} = .01, .05(.05).30$]

Figure 11c: Curves of λ = constant: keyhole [$\lambda = .1, .5, 1(1)10$]

Figure 12a: Critical curves: non-concentric cylinders [$\gamma = 1°, 5°(5°)85°$]

Figure 12b: Critical area-ratio curves: non-concentric cylinders [$A_{crit} = .01, .05(.05).20$]

Figure 12c: Curves of λ = constant: non-concentric cylinders [$\lambda = .1(.1).9$]

Figure 13: Generic corner.

Figure 14a: $\gamma = 30°$: acute corners critical.

Figure 14b: $\gamma = 60°$: acute corners critical.

Figure 14c: $\gamma = 30°$: obtuse corners critical.

Figure 14d: $\gamma = 30°$: all corners considered.

Figure 15: Decreasing β with α fixed: trapezoid.

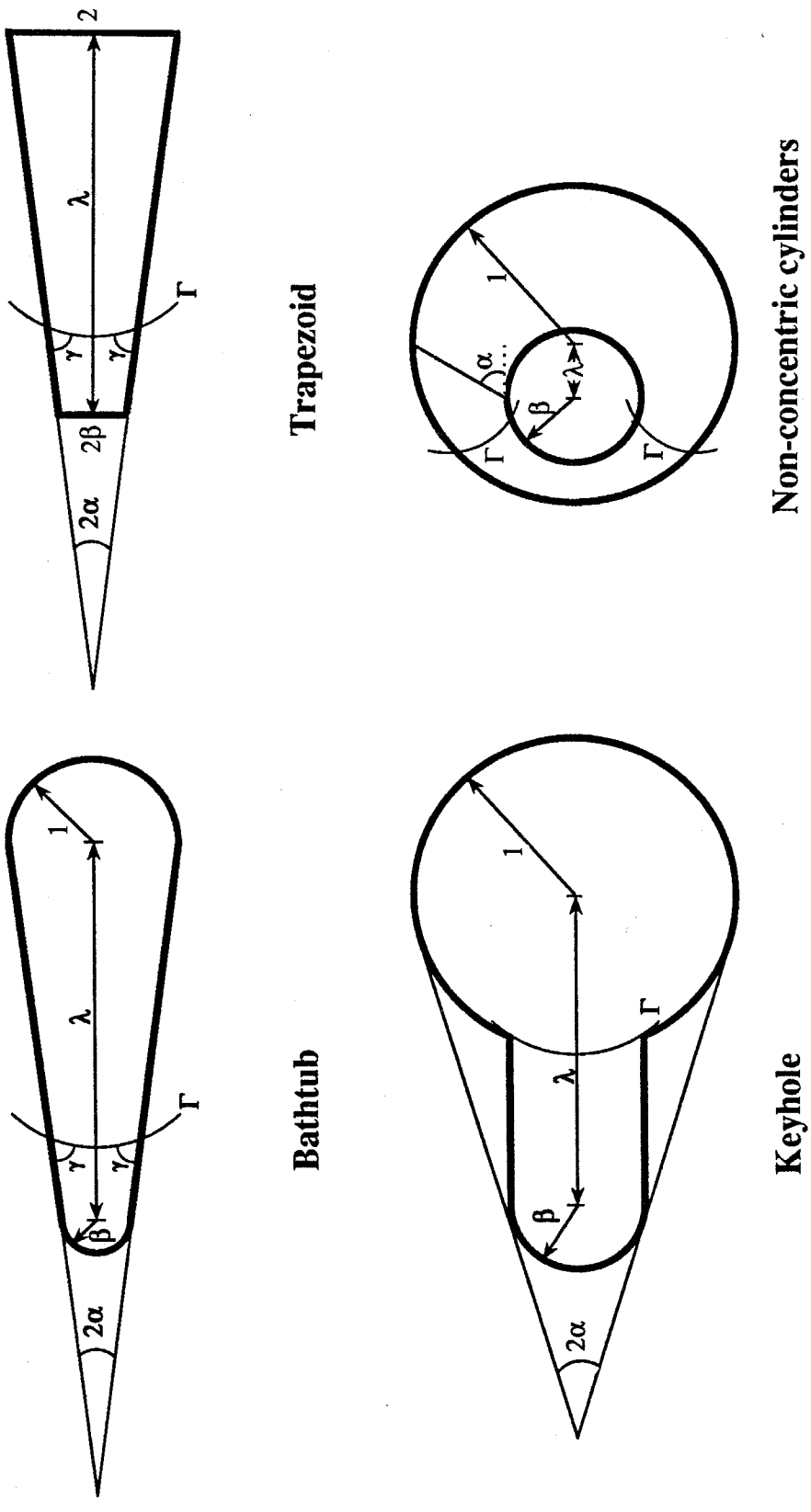

Figure 1 Four container cross sections

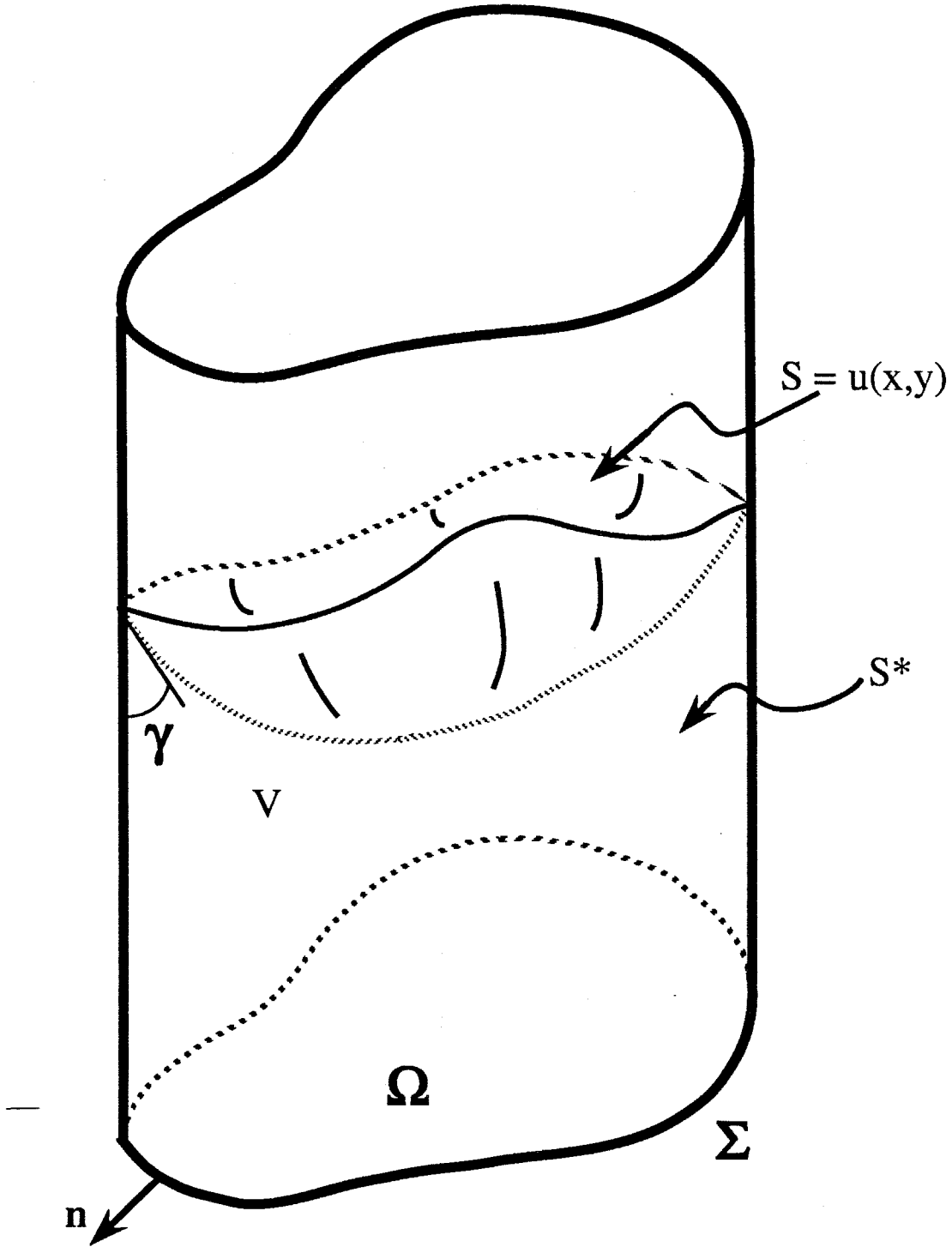

Figure 2 Generic cylinder

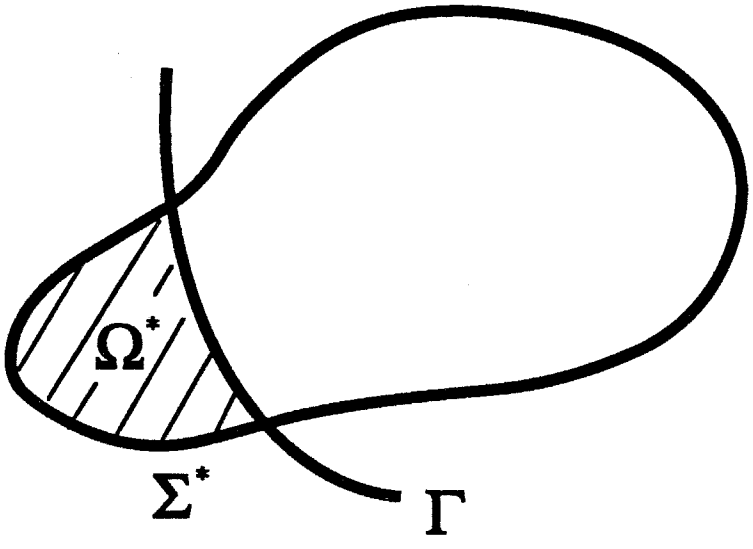

Figure 3 Cross section of generic cylinder

$$\Sigma = 2\,[\,\phi\beta + \frac{(1-\beta)}{\tan\alpha} + (\frac{\pi}{2} + \alpha)]$$

$$\Sigma^* = 2\,[\,\phi\beta + \frac{(T-\beta)}{\tan\alpha}]$$

$$\Omega = \phi\beta^2 + \frac{(1-\beta^2)}{\tan\alpha} + (\frac{\pi}{2} + \alpha)$$

$$\Omega^* = \phi\beta^2 + \frac{(T^2-\beta^2)}{\tan\alpha} - (\theta R_\gamma^2 - T\,R_\gamma \sin\gamma)$$

$$\theta = \frac{\pi}{2} - \alpha - \gamma \quad ; \quad \phi = \frac{\pi}{2} - \alpha$$

$$\lambda = \frac{(1-\beta)}{\sin\alpha}$$

$$\delta = \frac{(T-\beta)}{\tan\alpha}$$

$$T = \frac{R_\gamma \sin\theta}{\cos\alpha}$$

Figure 4a Φ terms: bathtub

$$\Sigma = 2\left[\ \beta + \frac{(1-\beta)}{\sin\alpha} + 1\ \right]$$

$$\Sigma^* = 2\left[\ \beta + \frac{(R_\gamma \sin\theta - \beta)}{\sin\alpha}\right]$$

$$\Omega = \frac{(1-\beta^2)}{\tan\alpha}$$

$$\Omega^* = \frac{(R_\gamma^2 \sin^2\theta - \beta^2)}{\tan\alpha} - (\theta - \sin\theta\cos\theta)\,R_\gamma^2$$

$$\theta = \frac{\pi}{2} - \alpha - \gamma$$

$$\lambda = \frac{(1-\beta)}{\tan\alpha}$$

$$\delta = \frac{R_\gamma \sin\theta - \beta}{\tan\alpha} - (1 - \cos\theta)\,R_\gamma$$

Figure 4b Φ terms: trapezoid

$$\Sigma = 2\left[\frac{\pi}{2}\beta + h + (\pi - \Theta)\right]$$

$$\Sigma^* = 2\left[\frac{\pi}{2}\beta + h\right]$$

$$\Omega = \frac{\pi}{2}\beta^2 + 2\beta h + (\pi - \Theta) + \beta\cos\Theta$$

$$\Omega^* = \frac{\pi}{2}\beta^2 + 2\beta h - (\theta R_\gamma^2 - \beta R_\gamma \cos\theta)$$

$$\theta = \arcsin\left(\frac{\beta}{R_\gamma}\right)$$

$$\Theta = \arcsin(\beta)$$

$$h = \lambda - \cos\Theta$$

Figure 4c Φ terms: keyhole, $h > 0$

$$\Sigma = 2\,[\,\phi\,\beta + (\pi - \Theta)]$$

$$\Sigma^* = 2\,\phi\,\beta$$

$$\Omega = \phi\,\beta^2 + (\pi - \Theta) + \lambda\,Y$$

$$\Omega^* = \phi\,\beta^2 - Y\,\beta\cos\,\phi - (\theta\,R_\gamma^2 - Y\,R_\gamma\cos\,\theta)$$

$$\theta = \arcsin\left(\frac{Y}{R_\gamma}\right) \quad ; \quad \phi = \arcsin\left(\frac{Y}{\beta}\right)$$

$$\Theta = \arcsin\,(Y)$$

$$Y = (1 - X^2)^{1/2} \quad ; \quad X = \frac{(1 + \lambda^2 - \beta^2)}{2\lambda}$$

(X,Y) = intersection of two circles: r = β; r = 1

For h > 0 and h < 0

$$\lambda = \frac{(1 - \beta)}{\sin\,\alpha}$$

Figure 4d Φ terms: keyhole, h < 0

$$\Sigma = 2\,[\,\pi\beta + \pi]$$

$$\Sigma^* = 2\,[\,\phi\beta + \Theta]$$

$$\Omega = -\pi\beta^2 + \pi$$

$$\Omega^* = \Theta - (X0)\,Y1 - (\lambda - X0)\,Y2 - \phi\beta^2 - 2\,(\theta R_\gamma^2 - D R_\gamma \cos\theta)$$

$$\theta = \arcsin\left(\frac{D/2}{R_\gamma}\right) \quad ; \quad \phi = \arcsin\left(\frac{Y2}{X2}\right)$$

$$\Theta = \arcsin\left(\frac{Y1}{X1}\right)$$

$$X0 = \frac{-b}{m} \quad ; \quad b = Y1 - m\,X1 \quad ; \quad m = \frac{Y1 - Y2}{X1 - X2}$$

(X1, Y1) = intersection of Γ and outer circle of radius 1

(X2, Y2) = intersection of Γ and inner circle of radius β

$$D = \frac{1}{2}\left((X1 - X2)^2 + (Y1 - Y2)^2\right)^{1/2}$$

$$\lambda = \frac{(1 - \beta)}{\tan\alpha}$$

Figure 4e Φ terms: non-concentric cylinders

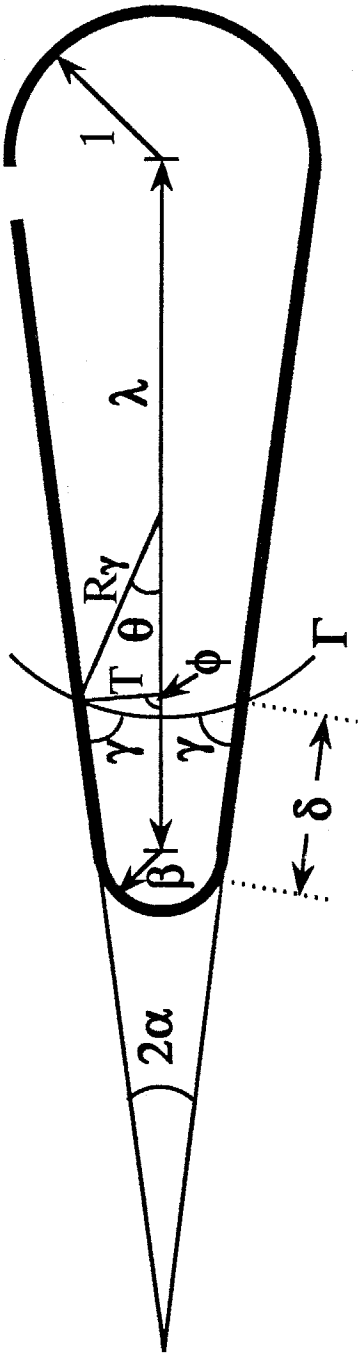

Figure 5 Bathtub

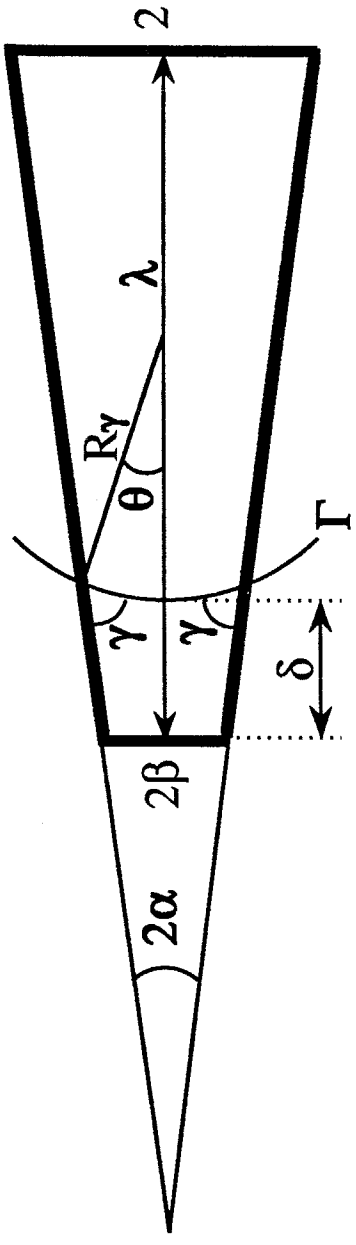

Figure 6 Trapezoid

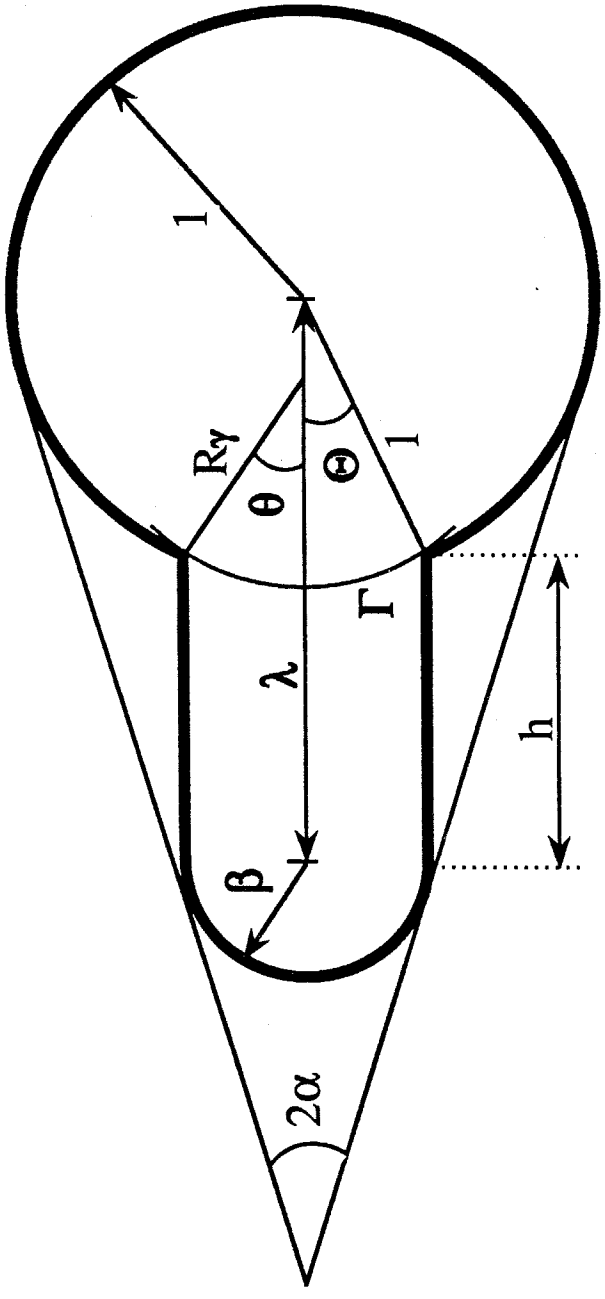

Figure 7a Keyhole, h > 0

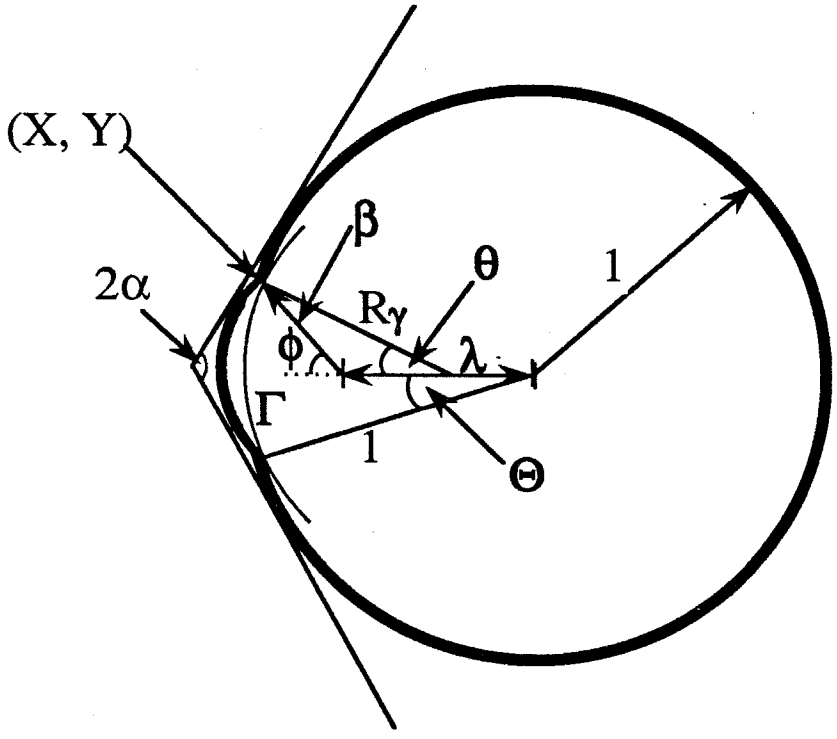

Figure 7b Keyhole, $h < 0$

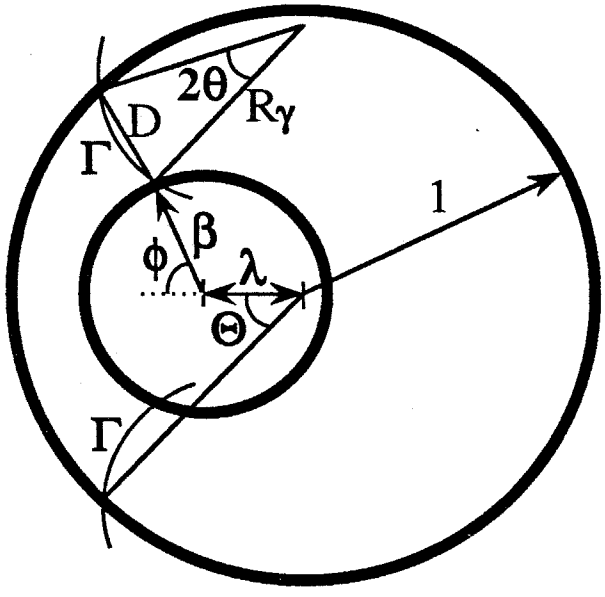

Figure 8a Non-concentric cylinders

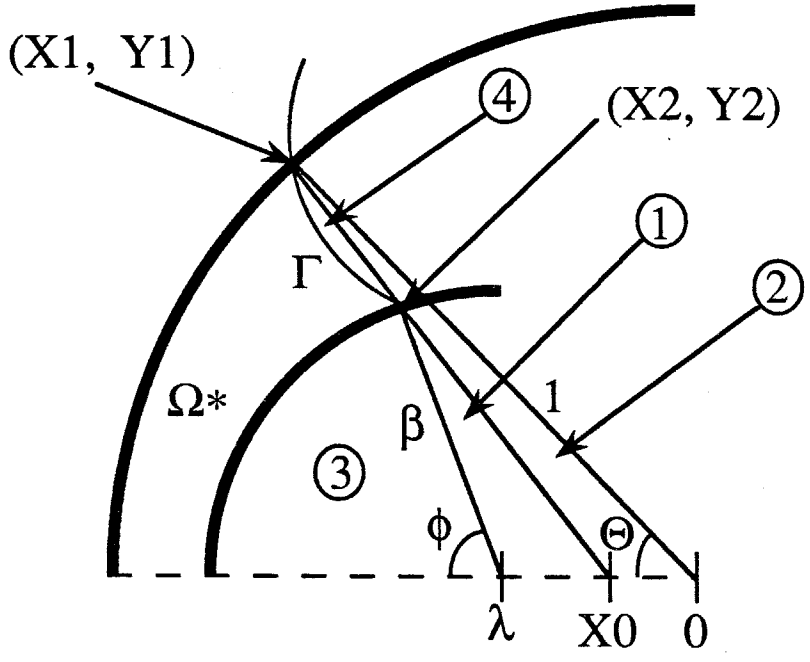

Figure 8b Non-concentric cylinders: detail of Ω*

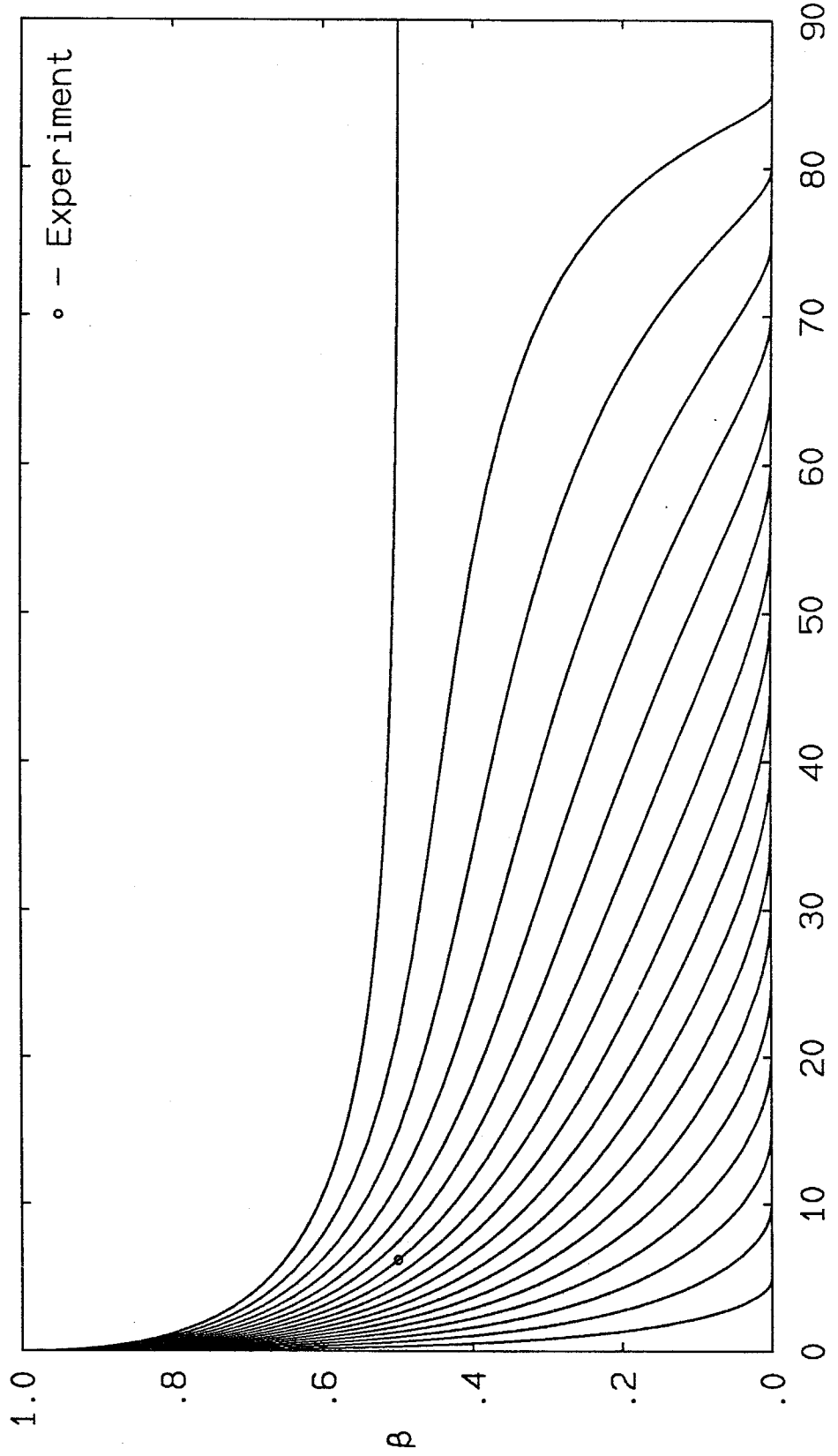

Figure 9a Critical curves: bathtub [γ=0(5)85 degrees]

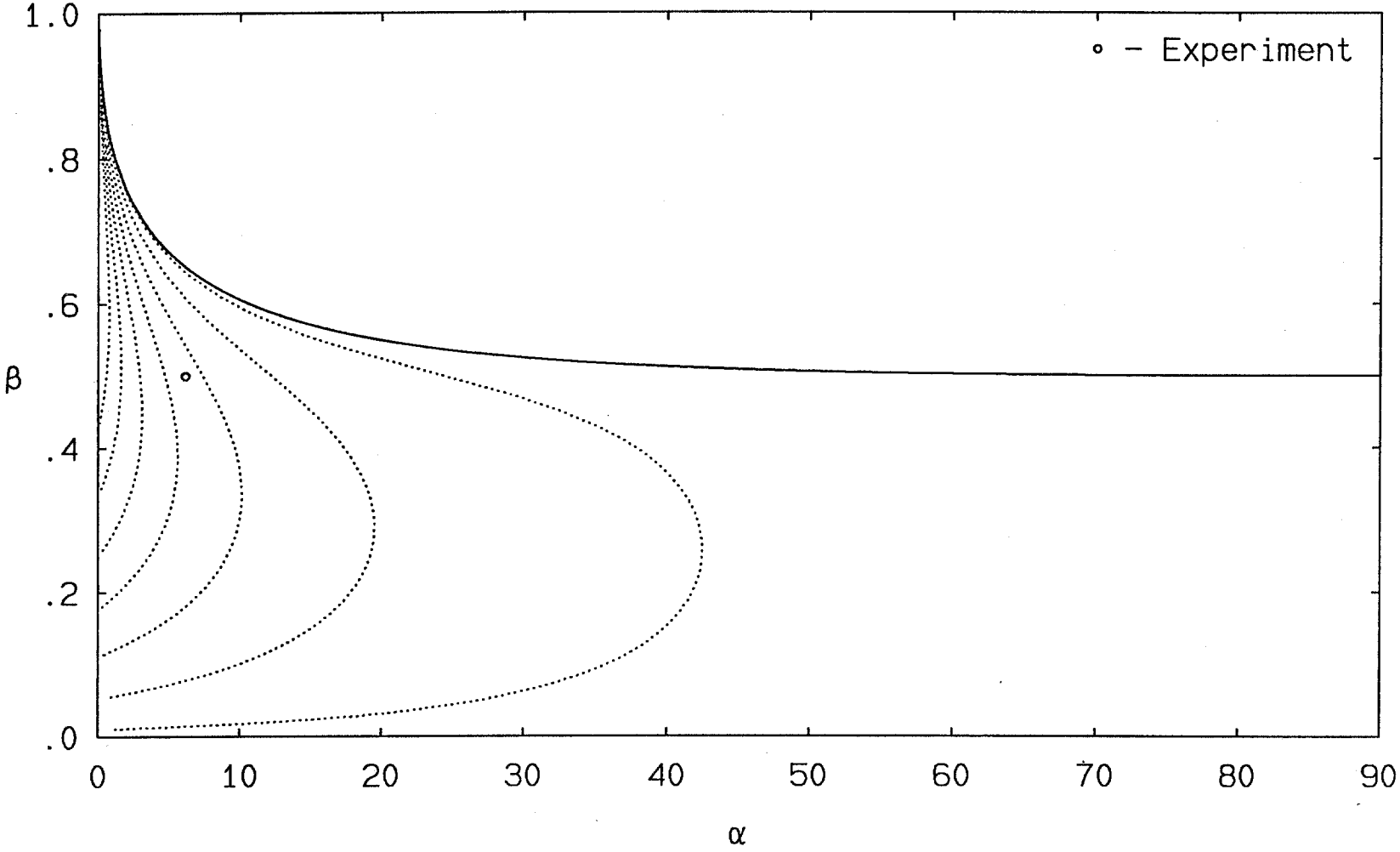

Figure 9b Critical area-ratio curves: bathtub [Acrit=.01,.05(.05).30]

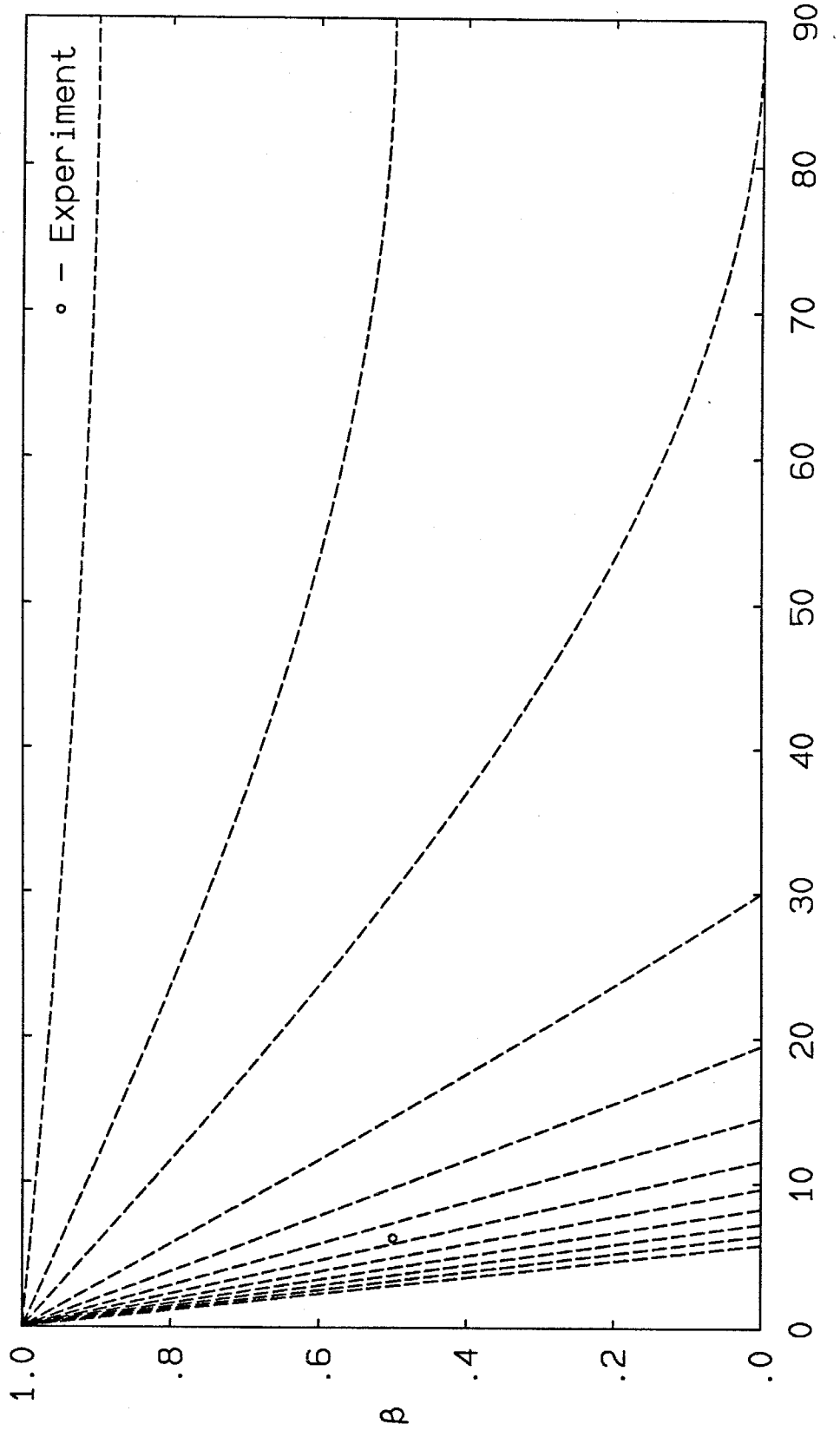

Figure 9c Curves of λ=constant: bathtub [λ=.1,.5,1(1)10]

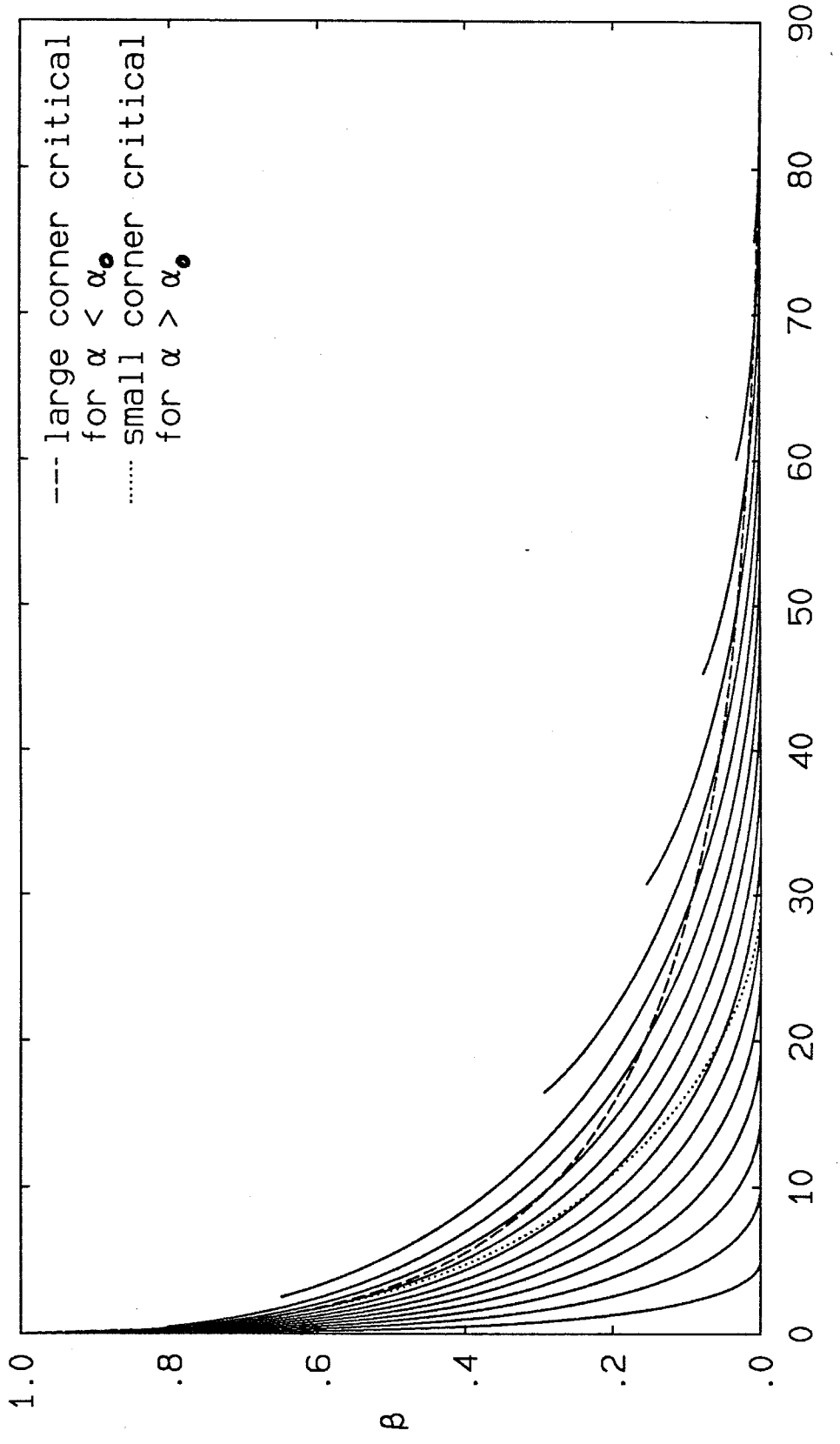

Figure 10a Critical curves: trapzoid [γ=0(5)85 degrees]

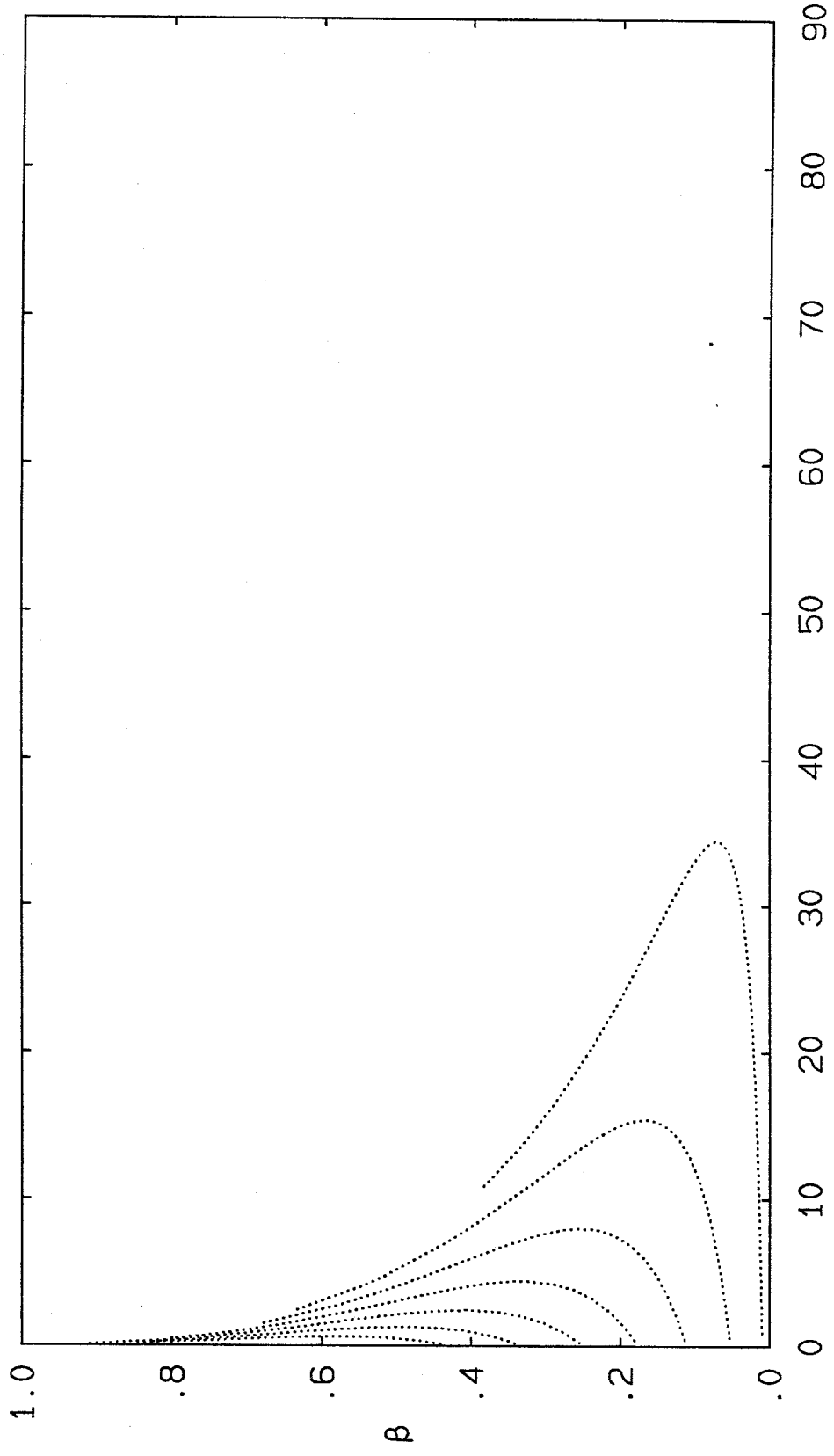

Figure 10b Critical area-ratio curves: trapezoid [Acrit=.01,.05(.05).30]

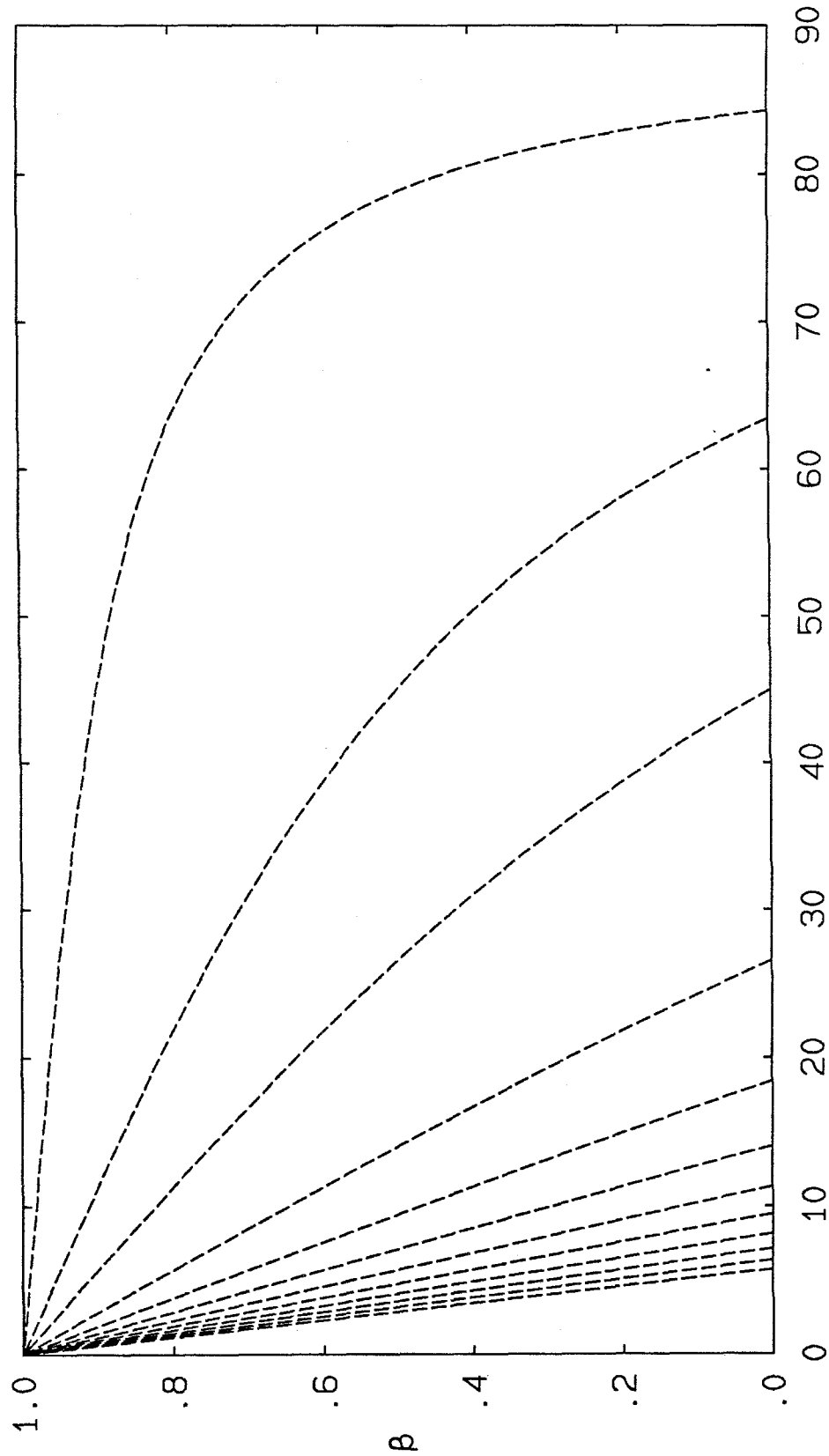

Figure 10c Curves of λ=constant: trapezoid [λ=.1,.5,1(1)10]

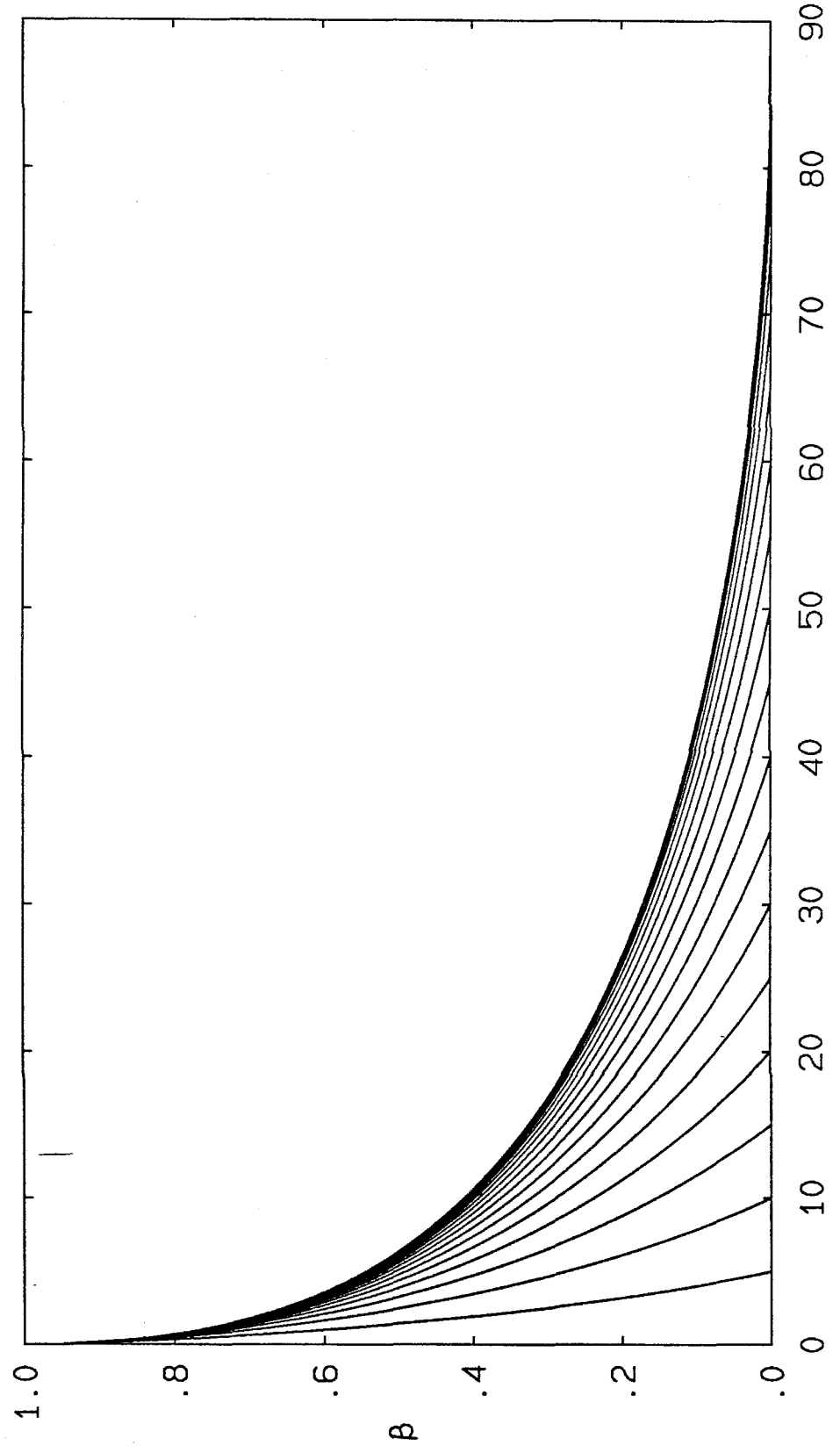

Figure 10d Curves of δ=0: trapzoid [γ=0(5)85 degrees]

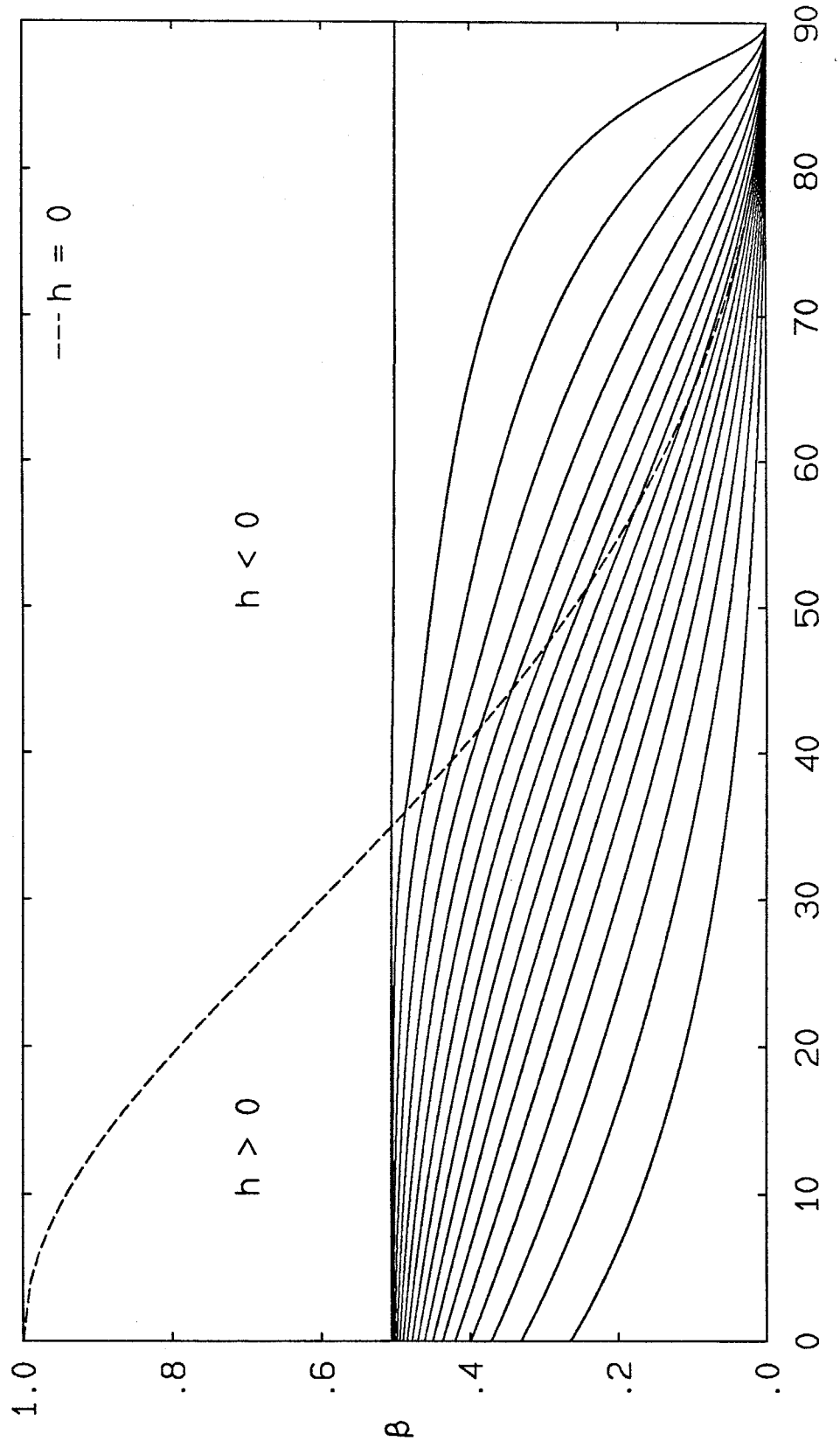

Figure 11a Critical curves: keyhole [γ=0(5)85 degrees]

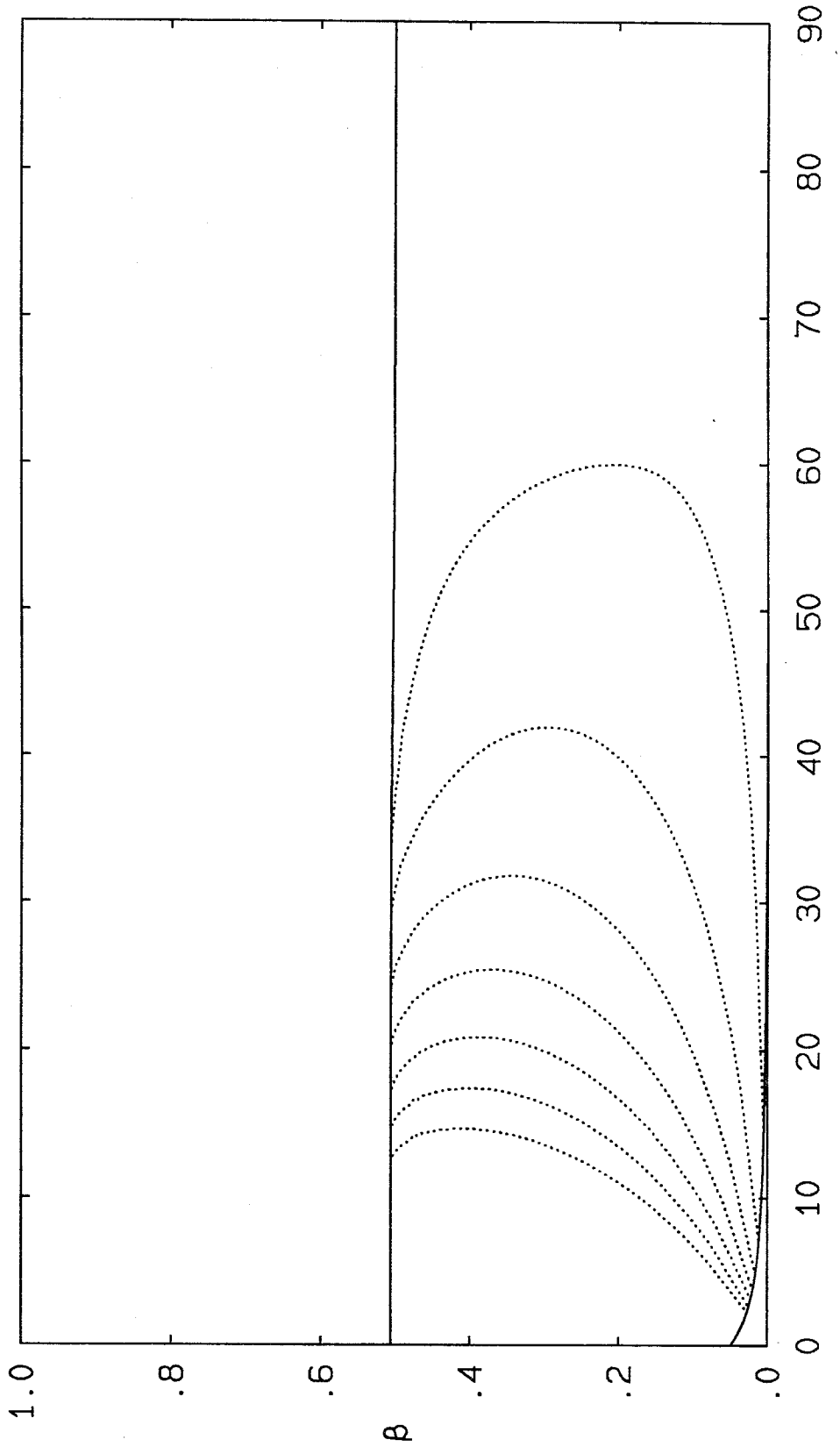

Figure 11b Critical area-ratio curves: keyhole [Acrit=.01,.05(.05).30]

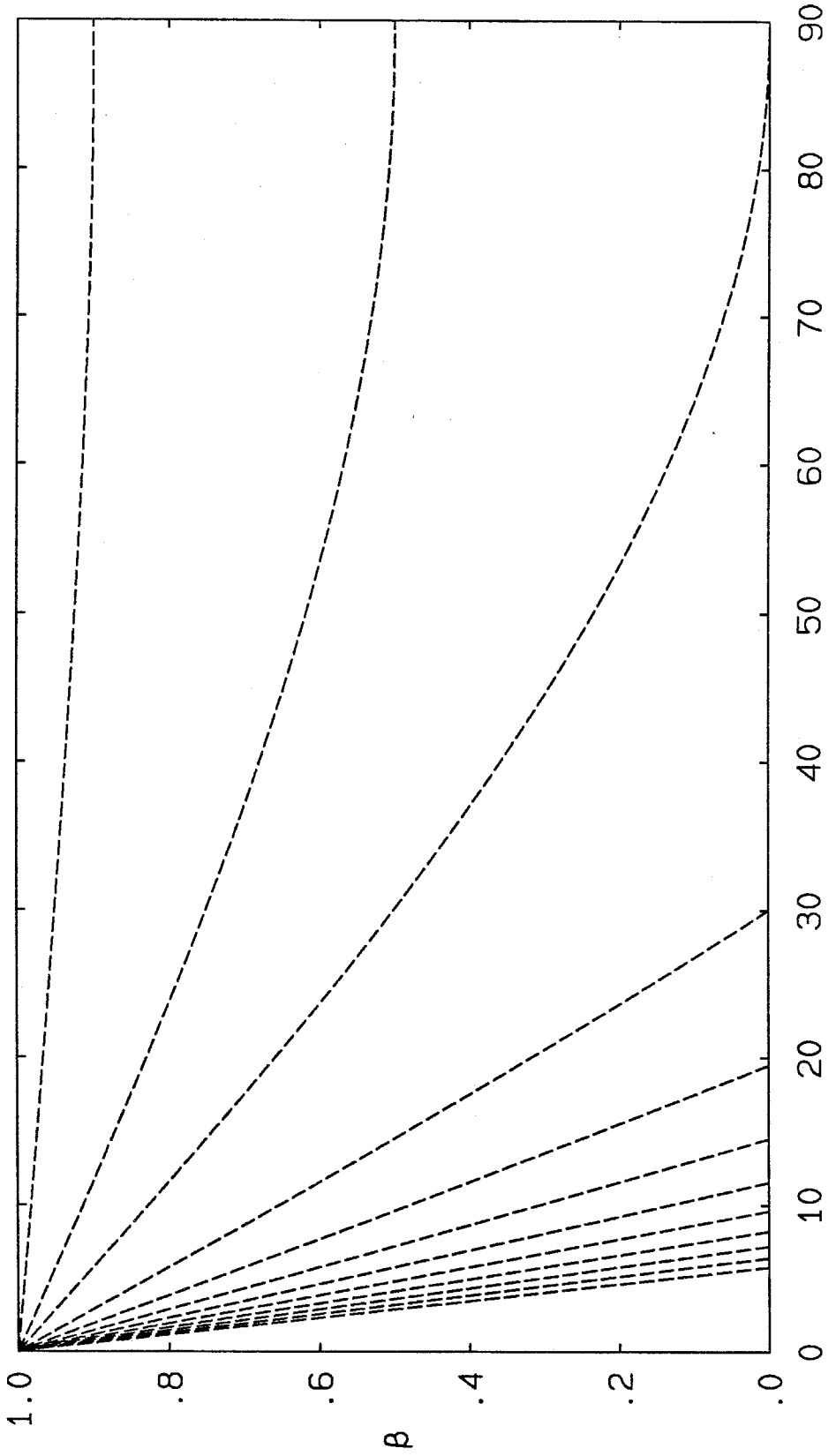

Figure 11c Curves of λ=constant: keyhole [λ=.1,.5,1(1)10]

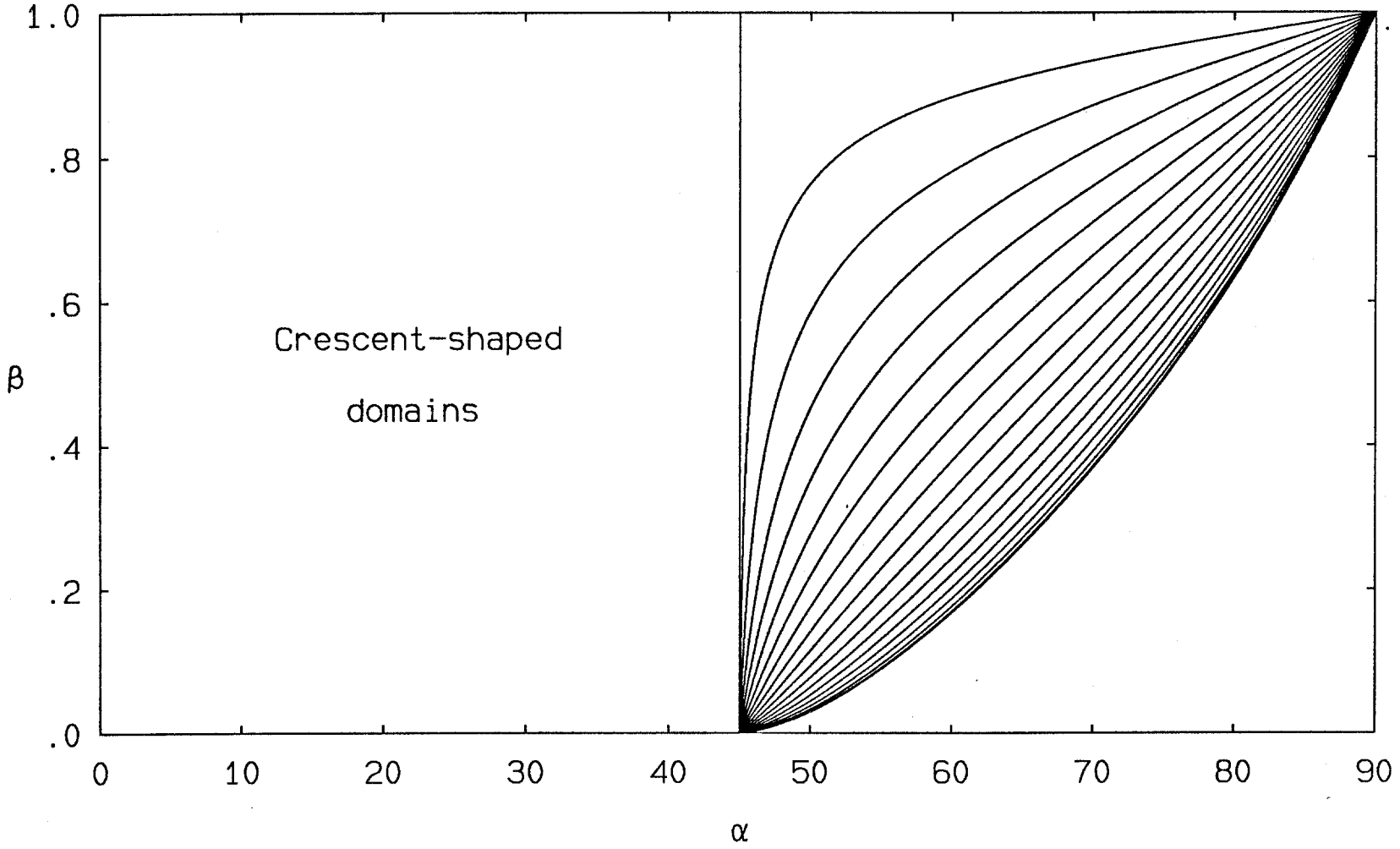

Figure 12a Critical curves: non-concentric cylinders
[γ=1,5(5)85 degrees]

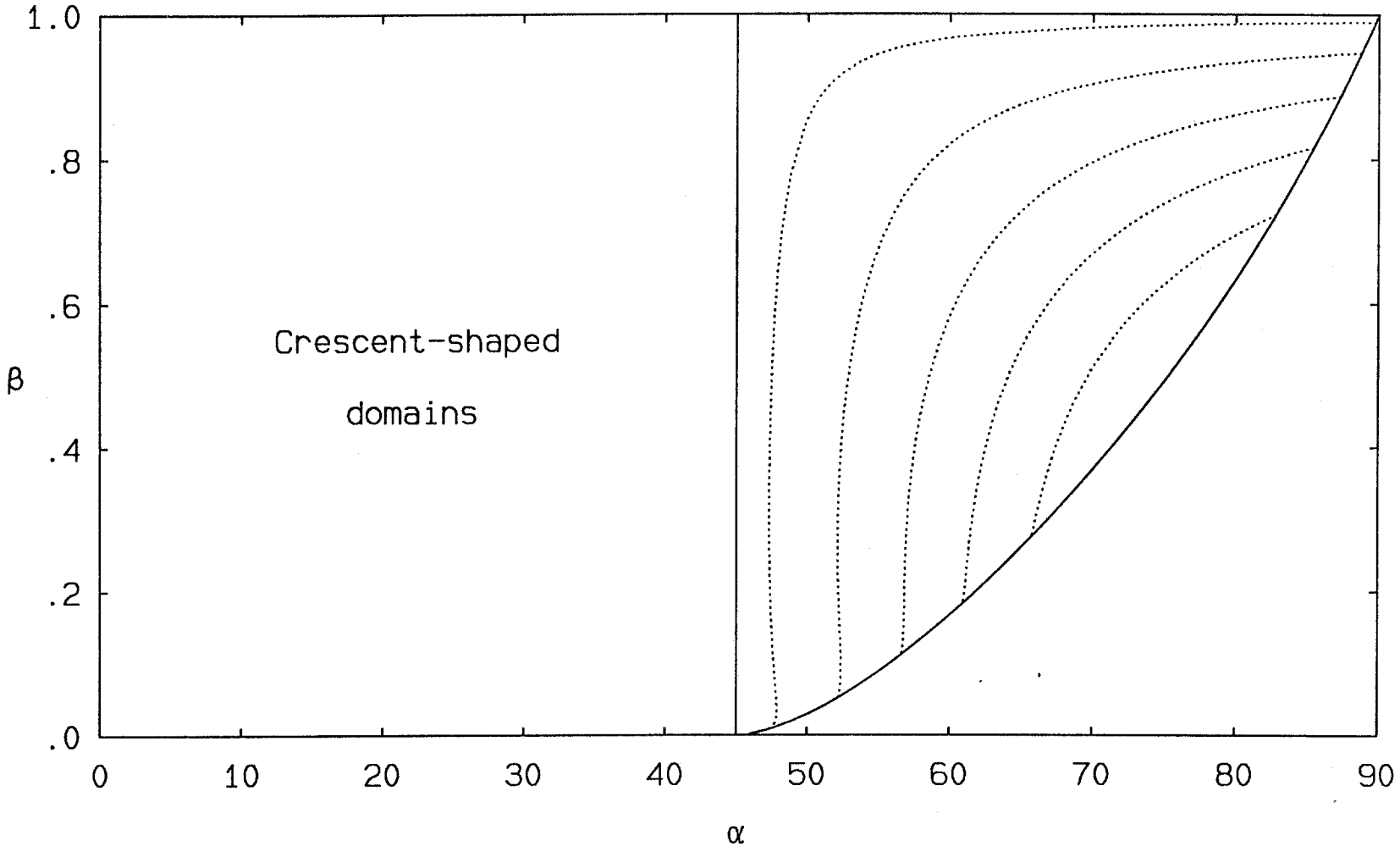

Figure 12b Critical area-ratio curves: non-concentric cylinders
[Acrit=.01,.05(.05).20]

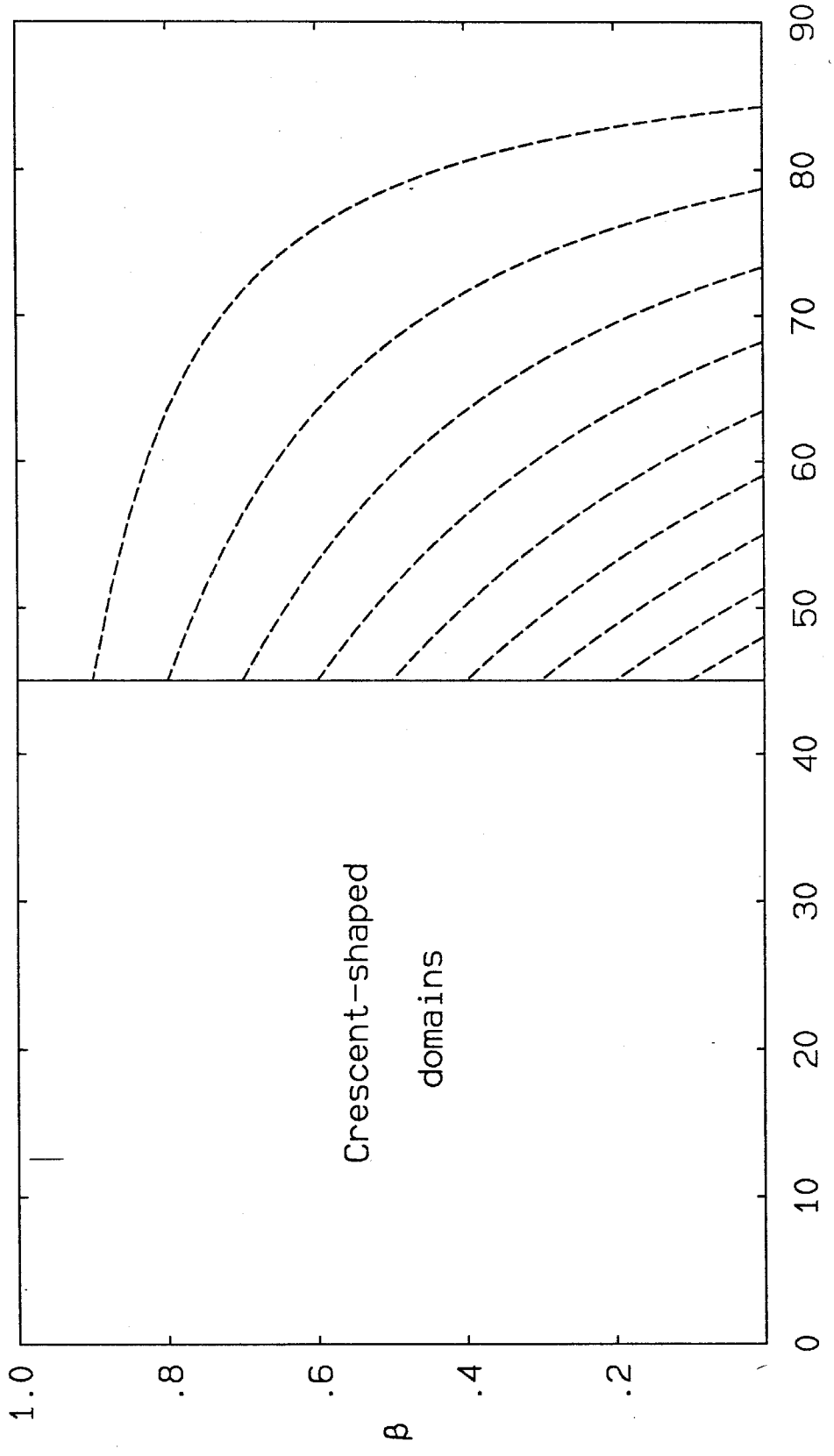

Figure 12c Curves of λ=constant: non-concentric cylinders
[λ=.1(.1).9]]

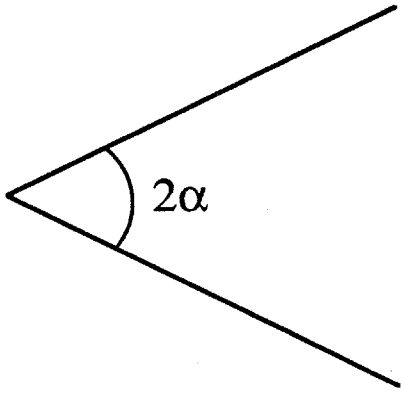

Figure 13 Generic corner

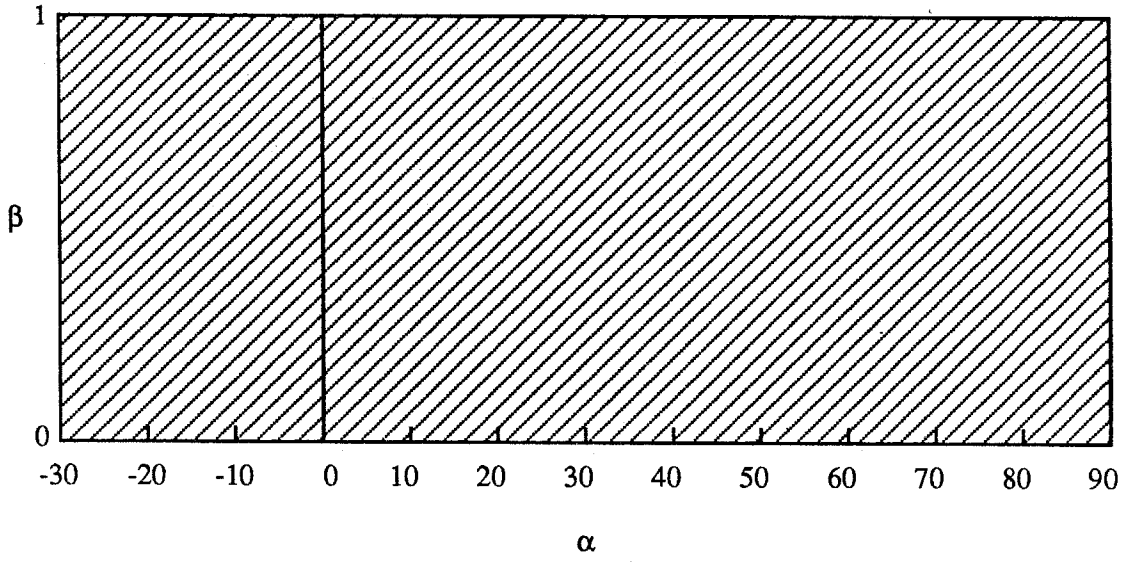

Fig 14a $\gamma = 30$ degrees
(acute corners critical)

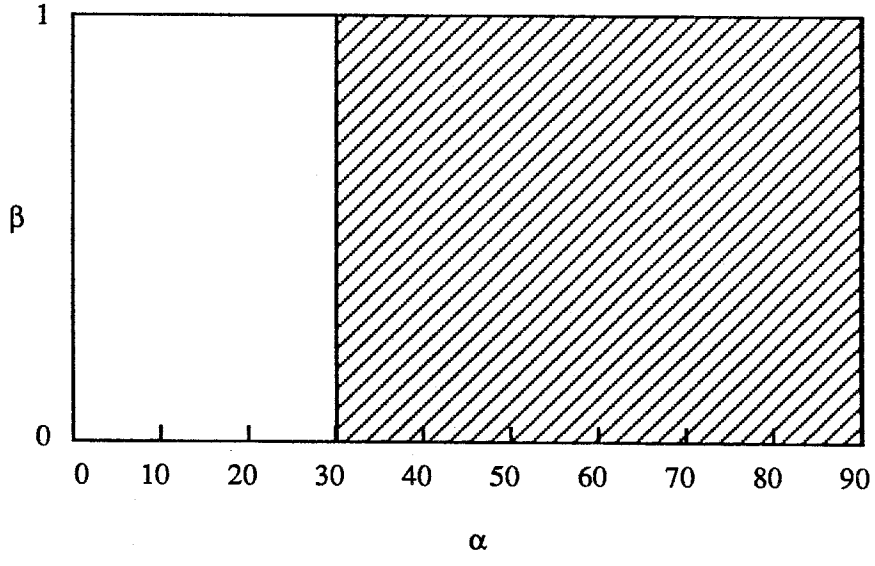

Fig 14b $\gamma = 60$ degrees
(acute corners critical)

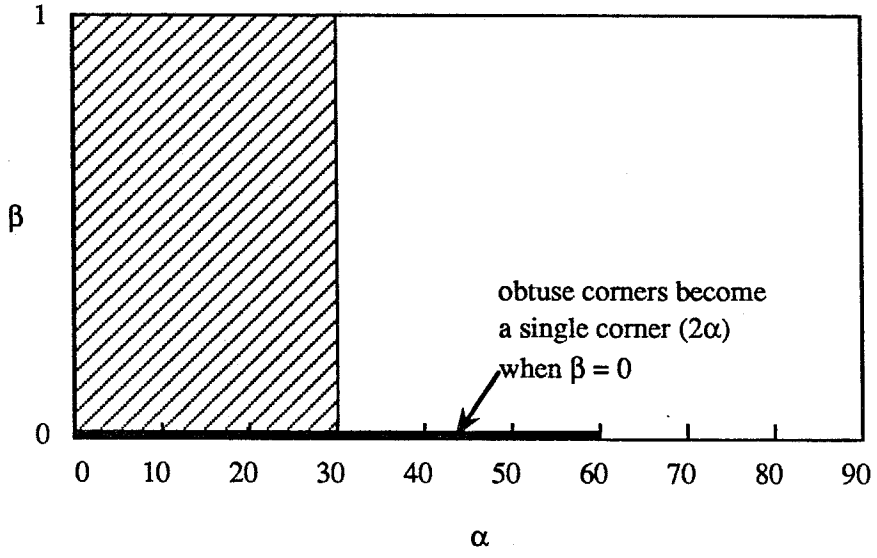

Fig. 14c $\gamma = 30$ degrees
(obtuse corners critical)

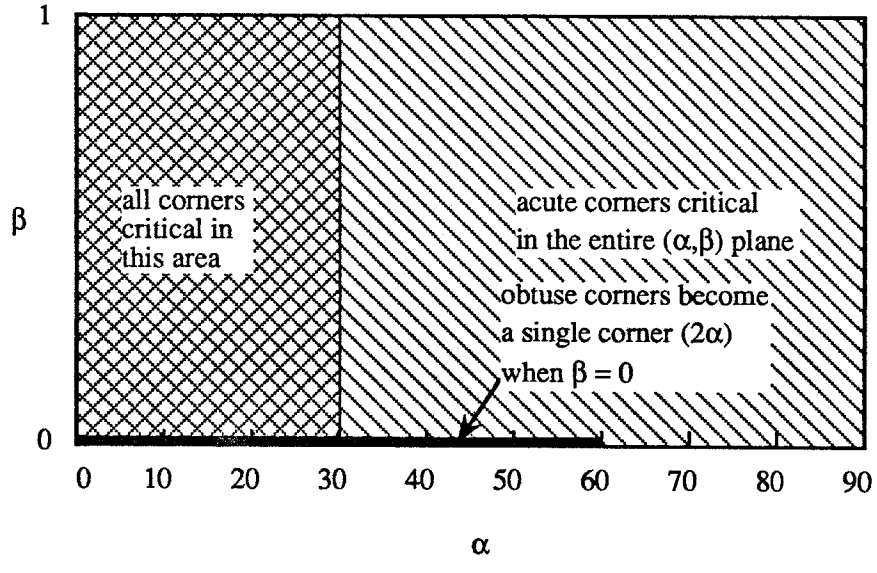

Fig. 14d $\gamma = 30$ degrees
(all corners considered)

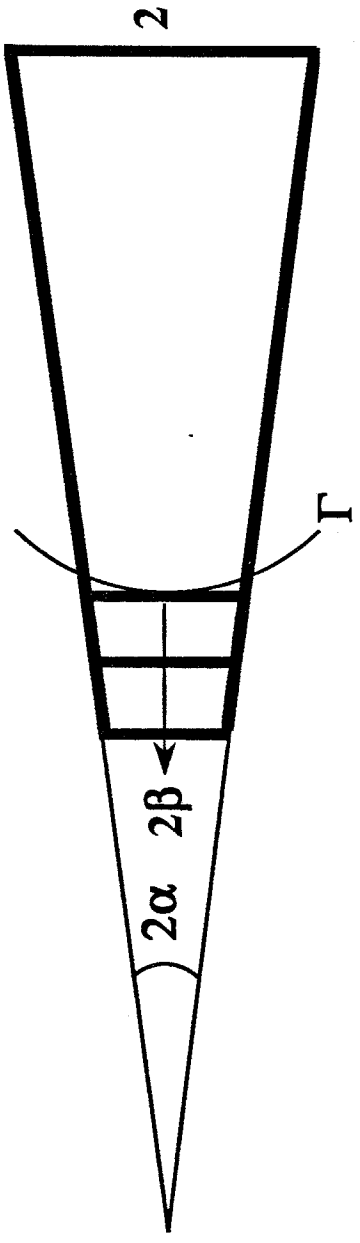

Figure 15 Decreasing β with α fixed: trapezoid

Table 1: Values of β-intercepts for various γ

γ	β
0	0.50647
5	0.50599
10	0.50462
15	0.50241
20	0.49940
25	0.49556
30	0.49089
35	0.48529
40	0.47867
45	0.47085
50	0.46159
55	0.45053
60	0.43715
65	0.42060
70	0.39954
75	0.37150
80	0.33137
85	0.26480
90	0.00000